CHALMERS
UNIVERSITY OF TECHNOLOGY

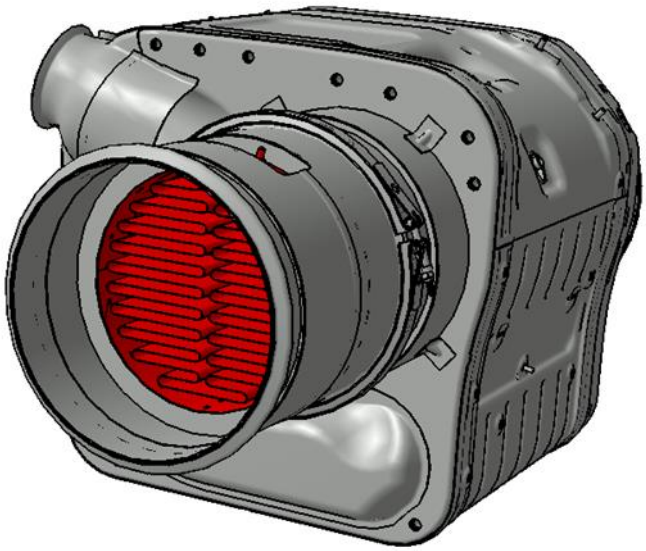

Evaluation of Electric Heater Performance in Exhaust Aftertreatment Systems

Master's thesis in Mobility Engineering

ATLIN ROY

DEPARTMENT OF MECHANICS AND MARITIME SCIENCES
CHALMERS UNIVERSITY OF TECHNOLOGY

Gothenburg, Sweden 2025
www.chalmers.se

MASTER'S THESIS IN MOBILITY ENGINEERING

Evaluation of Electric Heater Performance in Exhaust Aftertreatment Systems

ATLIN ROY

Department of Mechanics and Maritime Sciences
Division of Transport, Energy and Environment
CHALMERS UNIVERSITY OF TECHNOLOGY
Göteborg, Sweden 2025

Evaluation of Electric Heater Performance in Exhaust Aftertreatment Systems
ATLIN ROY

Supervisor: Swathy Suresh, SCANIA CV AB
Academic supervisor: Jonas Sjöblom, Department of Mechanics and Maritime Sciences
Examiner: Jonas Sjöblom, Department of Mechanics and Maritime Sciences

Department of Mechanics and Maritime Sciences
Division of Transport, Energy and Environment
Chalmers University of Technology
SE-412 96 Göteborg
Sweden
Telephone: + 46 (0)31-772 1000

Department of Mechanics and Maritime Sciences
Göteborg, Sweden 2025-09-21

Evaluation of Electric Heater Performance in Exhaust Aftertreatment Systems

Master's thesis in Mobility Engineering
ATLIN ROY
Department of Mechanics and Maritime Sciences
Division of Transport, Energy and Environment
Chalmers University of Technology

Abstract

Increasingly stringent vehicle emission standards call for improved performance of exhaust aftertreatment systems. A common problem is emissions during cold starts when the exhaust temperature is not sufficient to heat up the catalysts to operating conditions. Traditionally, this challenge is met by supplying additional exhaust heat using engine-based thermal management techniques by injecting additional fuel or decreasing engine efficiency. However, these techniques come with penalties such as increased fuel consumption and noise. An alternate solution is to use an electric heater to heat up the exhaust gases flowing into the catalysts. This can provide a large amount of heat close to the catalyst to enable them to reach operating temperatures quickly.

This study investigates the performance of an electric heater installed upstream of the silencer in a 380 hp 13-liter heavy-duty diesel engine. Tests in an air flow rig, an engine test cell were complemented with 1D simulations to evaluate catalyst heating performance, reduction of nitrogen oxides and energy consumed by the heater in steady and transient cycles. A major finding in this study was the effect of flow maldistribution limiting the effectiveness of the heater and the aftertreatment system. 1D models were found to be useful in testing different test cases but are challenged by flow maldistribution into the aftertreatment system.

The results show that a 10 kW heater works to improve nitrogen oxide emissions but need to be used in combination with engine modes that have low nitrogen oxide emissions. The performance of the system was also found to be significantly affected by the installation by heat losses in the exhaust flow.

Key words: engine, emissions, heater, exhaust, flow, maldistribution, nitrogen oxide, NO_X, catalyst

Contents

Abstract I
Contents II
Preface V
Notations VI
Table of Figures VIII
1 Introduction 1
1.1 Background 1
1.2 Purpose 2
2 Theory 3
2.1 Pollutants 3
2.2 Emission legislations 4
2.3 Emission control 6
2.3.1 Diesel Oxidation Catalyst (DOC) 6
2.3.2 Diesel Particulate Filter (DPF) 7
2.3.3 Selective Catalytic Reduction (SCR) 8
2.3.4 Ammonia Slip Catalyst (ASC) 9
2.4 Close-coupled SCR 9
2.5 Exhaust heating strategies 10
2.6 Electric heaters 12
2.7 Previous relevant work 14
3 Method 16
3.1 Aftertreatment system 16
3.1.1 Silencer 16
3.1.2 Heater 17
3.1.3 Sensors 19
3.2 Flow test 19
3.2.1 Test setup 19
3.2.2 Results 21
3.3 Engine test 27
3.3.1 Test setup 28
3.3.2 Results 31
3.4 1-D simulation 39
3.4.1 Setup 39
3.4.2 Results 41

3.5 Conclusions 48
3.6 Future work 50
4 References 51

Preface

This thesis was conducted at the exhaust aftertreatment department at Scania CV AB between January and June 2025. It evaluates an electric heater intended to improve cold-start exhaust aftertreatment performance. To this end, I combined experiments in an air-flow rig and an engine test cell with 1D simulations. This project gave me a chance to not just learn more about exhaust aftertreatment, but also to learn a bit more about defining questions, disciplined experimentation, and understanding my own approach at solving problems.

This work was made possible by the support of many people. I am grateful to Kim Petersson, the manager at Catalyst and Filter Performance, for the opportunity to combine physical testing, which I enjoy, with simulations, which I had long wished to try. Many thanks to my supervisors Swathy and Petra for their constant support and patience, and to the rest of the group for their inspiration and encouragement. I am also grateful to my colleagues in the neighbouring groups at Exhaust System Design and Performance, whose help I could rely on more times than I can count. I would like to thank my academic supervisor, Jonas Sjöblom, for his availability and guidance, which proved increasingly valuable as the project progressed.

Pierre Sabucco and Niklas Nordin helped me learn to use AVL Cruise and complemented my work with their own 3-D CFD simulations, helping me understand my test results better. Wolfgang and Anton the team at AVL were likewise generous with Cruise support. Ari Isomaa prepared the hardware that made my tests possible and never said no to a request. I am also grateful to my colleagues at Engine Development and Test Cell Operations for making the engine tests possible and helping me understand the results. I would also like to acknowledge Midhun Presannakumar without whom I wouldn't have found out about this opportunity to begin with. To the many others whose contributions are not listed here by name, please accept my sincere thanks.

Finally, to my family and friends: thank you for the encouragement and the reality checks.

Södertälje
2025-09-21

ATLIN ROY

Notations

Acronyms

1D	1 Dimensional
3D	3 Dimensional
ANR	Ammonia To NOX Ratio
ASC	Ammonia Slip Catalyst
ccSCR	Close-Coupled Selective Catalytic Reduction
CDA	Cylinder Deactivation
CFD	Computational Fluid Dynamics
DC	Direct Current
DEF	Diesel Exhaust Fluid
DOC	Diesel Oxidation Catalyst
DPF	Diesel Particulate Filter
EH	Electric Heater
EMS	Engine Management System
EPA	Environmental Protection Agency
EU	European Union
EVO	Exhaust Valve Opening
FC	Fuel Consumption
FTIR	Fourier Transform Infrared Spectroscopy
FTP	Federal Test Procedure
GHG	Greenhouse Gas
HC	Hydrocarbons
ISC	In-Service Conformity
IVO	Intake Valve Opening
NOX	Nitrogen Oxides
PC	Personal Computer
PM	Particulate Matter
PTC	Positive Temperature Coefficient
RDE	Real Driving Emissions
SCR	Selective Catalytic Reduction
TM	Thermal Management
UI	Uniformity Index
USB	Universal Serial Bus
VVT	Variable Valve Timing
WHSC	World Harmonized Stationary Cycle
WHTC	World Harmonized Transient Cycle

Chemical Species

C	Carbon
CH_4	Methane
CO	Carbon monoxide
CO_2	Carbon dioxide
H_2O	Water
N_2	Nitrogen
N_2O	Nitrous oxide
NH_3	Ammonia
NO	Nitric oxide
NO_2	Nitrogen dioxide
O_2	Oxygen

Greek letters

η_h	Heater thermal Efficiency
$\overline{\phi_a}$	Area-weighted average of flow variable
ϕ_i	Measured value of flow variable at face i
γ_a	Uniformity index

English symbols

A_i	Area of face i
P	Power
U	Voltage
R	Resistance
T	Temperature
C_p	Specific heat capacity
$\dot{m}$	Mass flowrate

Table of Figures

Figure 2.1 Relative concentration of pollutant emissions in diesel exhaust gas (Majewski, 2024b) 3
Figure 2.2 Euro 1-6 emission limits for PM and NO_X from heavy-duty vehicles 4
Figure 2.3 Current and future heavy-duty emissions regulations 5
Figure 2.4 Euro 6 compliant heavy-duty diesel aftertreatment system layout (2021) 6
Figure 2.5 Monolithic catalyst substrates (Majewski, 2022) 6
Figure 2.6 Wall-flow and flowthrough substrates: Flow pattern (Majewski, 2020) 7
Figure 2.7 SCR temperature and NO_X during the cold FTP-75 cycle 9
Figure 2.8 Two possible ccSCR layouts (The Danish Environmental Protection Agency, 2021) 10
Figure 2.9 Structure of a rolled electric heater (Li et al., 2024) 13
Figure 2.10 HJS heater band (Lindemann et al., 2022) 13
Figure 3.1 Layout of aftertreatment system with heater 16
Figure 3.2 Silencer with heater and diffuser cone 16
Figure 3.3 Original and modified silencer inlets 17
Figure 3.4 Heater during tests at supplier 17
Figure 3.5 Maximum heater power vs temperature 18
Figure 3.6 Maximum allowed heater power vs exhaust gas temperature 18
Figure 3.7 Silencer and heater installation in air flow rig 19
Figure 3.8 Thermocouple grid after heater 20
Figure 3.9 SCR1 thermocouples in flow rig test 20
Figure 3.10 Temperature distribution 70 mm downstream of heater 21
Figure 3.11 Maximum temperature at TS_SCR1_1 22
Figure 3.12 Heat losses at TS_SCR1_1 22
Figure 3.13 Time for 50 K increase at TS_SCR1_1 23
Figure 3.14 Rise rate for 50 K increase at TS_SCR1_1 23
Figure 3.15 SCR1 temperature distribution at 200 kg/h and 8 kW 24
Figure 3.16 SCR1 temperature distribution at 500 kg/h and 8 kW 24
Figure 3.17 Axial velocity and temperature distributions at 200 kg/h 25
Figure 3.18 Axial velocity and temperature distributions at 500 kg/h 25
Figure 3.19 Position of thermocouples for testing radiative error 26
Figure 3.20 Temperature rise at thermocouples for testing radiative error 27
Figure 3.21 Silencer and heater installation in engine test rig 28
Figure 3.22 SCR1 and DPF thermocouples in engine test 29
Figure 3.23 Mixer installed upstream of diffuser inlet 30
Figure 3.24 Heater power control flowchart 30
Figure 3.25 Relative temperature ratios at 300 kg/h and 8 kW with mixer 31
Figure 3.26 Relative temperature ratios at 300 kg/h and 8 kW without mixer 31
Figure 3.27 Relative temperature ratios at 600 kg/h and 8 kW with mixer 32
Figure 3.28 Relative temperature ratios at 600 kg/h and 8 kW without mixer 32
Figure 3.29 Time, engine-out NO_X and fuel consumed until start of dosing in cold WHTC 33
Figure 3.30 Temperature trace for 600s of cold WHTC 34
Figure 3.31 Energy flow between turbocharger outlet and SCR1 inlet for 74s of cold WHTC 34

Figure 3.32 Energy flow between turbocharger outlet and SCR1 inlet in cold WHTC 35
Figure 3.33 Engine-out NO_X, tailpipe NO_X and fuel consumed in cold WHTC 35
Figure 3.34 Time, engine-out NO_X and fuel consumed until start of dosing in LLC 36
Figure 3.35 Engine-out NO_X, tailpipe NO_X and fuel consumed in LLC 37
Figure 3.36 Time, engine-out NO_X and fuel consumed until start of dosing at idle 38
Figure 3.37 Engine-out NO_X, tailpipe NO_X and fuel consumed at idle 38
Figure 3.38 Comparison of tailpipe NO_X in test and simulation for cold WHTC ..41
Figure 3.39 Comparison of tailpipe NO_X and heater energy consumption with and without diffuser for cold WHTC.....42
Figure 3.40 Comparison of tailpipe NO_X with different heater strategies for cold WHTC 43
Figure 3.41 Comparison of heater energy consumption with different heater strategies for cold WHTC 43
Figure 3.42 Comparison of tailpipe NO_X in test and simulation for LLC 44
Figure 3.43 Comparison of tailpipe NO_X and heater energy consumption with and without diffuser for LLC.....44
Figure 3.44 Comparison of tailpipe NO_X and heater energy consumption with different heater strategies for LLC.....45
Figure 3.45 Comparison of tailpipe NO_X in test and simulation for idle.....46
Figure 3.46 Comparison of tailpipe NO_X and heater energy consumption with and without diffuser for idle 46
Figure 3.47 Comparison of tailpipe NO_X and heater energy consumption with different heater strategies for idle 47

1 Introduction

1.1 Background

Heavy-duty road vehicles (medium- and heavy-duty trucks, buses and coaches) are responsible for nearly 30% of road transport green-house gas (GHG) emissions (212 Mt CO_2eq/year in 2019), accounting for 6% of overall EU GHG emissions (Shirizadeh et al., 2024). The decarbonization of heavy-duty road transport is subject to many uncertainties regarding fuel choices and policy decisions, and projections for electrified road transport are varied (Shirizadeh et al., 2024). Even in the most ambitious environment for electrification there exists a robust role for other vehicle-fuel options . Hence, reduction of combustion engine exhaust emissions remains a priority. Besides contributing to global warming, pollutants in exhaust gases are also a hazard to environmental and human health. The most significant harmful products are carbon monoxide (CO), hydrocarbons (HC), nitrogen oxides (NO_X), and particulate matter (PM) (Reşitoğlu et al., 2014). Road transport accounts for 40-70 % of urban NO_X emissions worldwide.

The evolution of vehicle emission standards has significantly impacted global air quality over the past decades. The progression from Euro 1 to Euro 6 standards, along with similar regulations in other regions, has led to substantial reductions in CO, HC, NO_X, and PM emissions (Ravi et al., 2023). These improvements have been achieved through technological advancements in engine efficiency and aftertreatment systems. However, newer regulations with stricter limits focus on minimizing emissions over extensive on-road operating conditions, especially in urban driving and cold-start operation.

Conventional aftertreatment methods have poor efficiency at low temperatures. To increase exhaust temperature rapidly, engine-based heating strategies are commonly used. However, these methods often increase fuel consumption and emissions. Electric heating of the exhaust gas is a potential solution to address the challenges associated with cold starts and low-load operation that Scania is interested in investigating further.

1.2 Purpose

The aim of this thesis is to understand the feasibility of using an electric heater as a thermal management option for the exhaust aftertreatment system of a heavy duty truck. This will be done using 1D simulations of an electric heater added to an existing aftertreatment model, physical flow tests with an electric heater and aftertreatment system, and tests in an engine test cell. The process and results will be documented to serve as methodology for improved development of the aftertreatment system.

The primary objectives are:

- Determine the maximum heater power required and time to catalyst light-off using simulations and flow test.
- Determine energy required for quick light-off and staying above the required SCR inlet temperature during cold start and low load operation.
- Determine a control strategy to optimize heater power usage.

The secondary objectives are:

- Find the temperature uniformity of the gas flow across the heater from the flow test.
- Determine fuel consumption and tailpipe NO_X emissions if the energy used to power the heater is provided by the engine.

2 Theory

2.1 Pollutants

Diesel engine exhaust primarily contain N_2, CO_2, H_2O and O_2, along with a small proportion of. Although the relative concentration of the pollutants in the exhaust gas is about a tenth of the volume, they are potent and have been a major concern for public health and climate change.

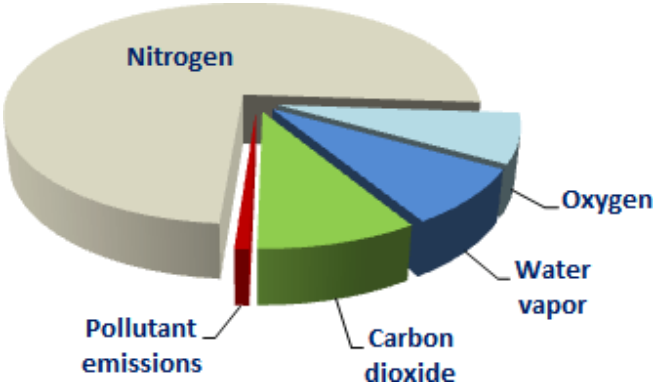

Figure 2.1 Relative concentration of pollutant emissions in diesel exhaust gas (Majewski, 2024b)

The main pollutants are:

- Nitrogen oxides (NO_X)
  NO_X is a mixture of nitric oxide (NO) and nitrogen dioxide (NO_2).
  NO is the major component of these NO_X emissions and is primarily formed by oxidation of N_2 at high temperatures in the combustion chamber through the Zeldovich mechanism. NO can subsequently be oxidized to NO_2 especially at lean conditions.

  NO released into the atmosphere reacts with ozone to form NO_2. NO_2 exposure is linked to respiratory issues and diseases. It also contributes to acid rain, and reacts with volatile organic compounds to form ozone and smog.

- Particulate matter (PM)
  PM, formed from soot, can cause respiratory problems, cancer and cardiovascular diseases.

- Hydrocarbons (HC)
  HC emissions are respiratory tract irritants, carcinogenic, ozone precursors and contribute to smog.

- Carbon monoxide (CO)
  CO is highly toxic to humans, and can cause loss of consciousness and death.

- Carbon dioxide (CO_2)
  CO_2 is a major contributor to global warming.

- Methane (CH_4)
  CH_4 is a major contributor to global warming.

- Nitrous oxide (N_2O)
  N_2O is a major contributor to global warming.

Of these, the most problematic ones are considered to be NO_X and PM. Diesel engines are responsible for about 85 % of all the NO_X emissions from mobile sources (Reşitoğlu et al., 2014).

2.2 Emission legislations

Emission legislations all over the world have been enforced beginning in the early 90s to regulate the maximum amount of pollutants from vehicles. These legislation limits have been lowered with every update forcing vehicle manufacturers to develop advanced engine and emission control technology.

The European emission standards started with Euro 1 in 1992 and Euro 6 is currently in use. There are three sets of emission standards – steady state, transient , and real driving emissions (RDE) testing. Two test cycles – a hot start steady state cycle called the World Harmonized Stationary Cycle (WHSC), and a transient cycle called the World Harmonized Transient Cycle (WHTC) with both cold and hot start requirements are used for standardized tests for emissions.

For better evaluation of emissions from real world driving, off-cycle emissions are also tested for type approval. After the vehicle enters service, other requirements are in-service conformity (ISC) tests, on-board diagnostics measures to ensure the aftertreatment system is working as required and manufacturers should demonstrate that the emission values are within limits for the useful life of the vehicle.

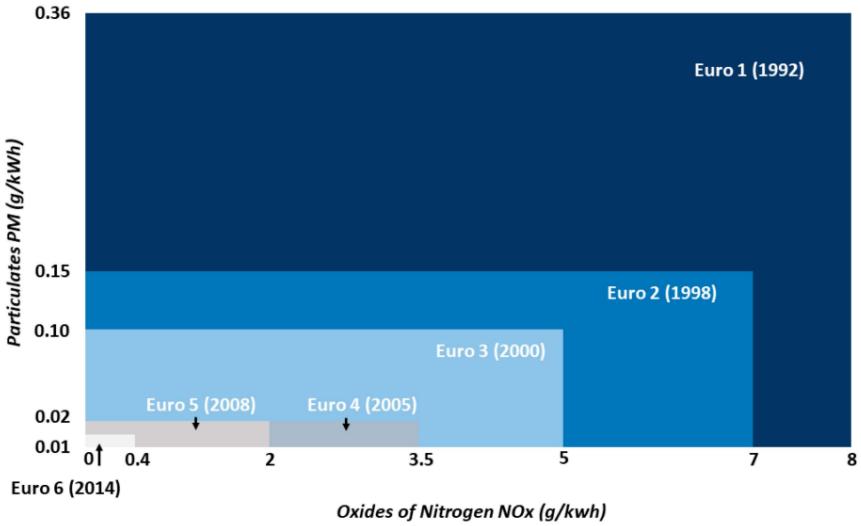

Figure 2.2 Euro 1-6 emission limits for PM and NO_X from heavy-duty vehicles

The limits for PM and NO_X emissions for heavy duty vehicles were reduced from Euro 1 to Euro 6 by 97 and 95% as shown in Figure 2.2 (Ravi et al., 2023). With the

upcoming Euro 7 legislation, the limits are made stricter. Some of the most important differences are:

- PM and NO_X limits for heavy-duty diesel vehicles will be reduced further by 20% and 50% as shown in Figure 2.3 (Infineum Insight, 2024).
  Particle numbers (PN) measured will be for a smaller particle size.
- Limits for N_2O emissions are introduced.
- For real driving emissions (RDE), the conformity factor for pollutants, and power threshold for assessing which windows of test data are to be evaluated, have been reduced. This capture more low-load and low-speed operation.
- The durability period for which vehicles must comply with the emission limits have been increased.

Emission limits (mg/kWh unless noted)	Euro VI petrol	Euro VI diesel	
	Euro VI Transient testing	Euro VI Transient testing	Euro VI Steady-state testing
NOx	460	460	400
PM	10	10	10
PN_{23nm} (#/kWh)	6.0×10^{11}	6.0×10^{11}	8.0×10^{11}
CO	4000	4000	1500
THC	–	160	130
NMHC	160	–	–
NH_3 (ppm)	10	10	10
CH_4	500	–	–

Emission limits (mg/kWh unless noted)	Euro 7	
	WHSC (CI) & WHTC (CI&PI)	RDE
NOx	200	260
PM	8	–
PN_{10nm} (#k/Wh)	6×10^{11}	9×10^{11}
CO	1500	1950
NMOG	80	105
NH_3 (ppm)	60	85
CH_4	500	650
N_2O	200	260

Figure 2.3 Current and future heavy-duty emissions regulations

Upcoming emission standards in some markets place additional demands on NO_X emissions during idle. In the United States, where trucks frequently idle overnight to power 'hotel loads' (air conditioning, lighting, radio, refrigerator etc.), the 2027 Environmental Protection Agency (EPA) rule sets a clean idle NO_X limit of 10 g/h. For an average hotel load of 5 kW in a long-haul truck (Brodrick et al., 2001), this is equivalent to a NO_X limit of 2 g/kWh which is ten times higher than the WHTC limit. In Europe, hoteling by idling is not very prevalent

Euro 7 does not include a specific idle NO_X limit because hoteling by idling overnight is not as prevalent as in the US. But emissions from idle are indirectly included in RDE tests if it is inside a valid test window where average power ≥ 6 % of the engine's rated power (eg., stop-and-go driving).

2.3 Emission control

A modern diesel engine aftertreatment system typically consists of at least:

- a diesel oxidation catalyst (DOC), to oxidize unburnt hydrocarbons and CO to carbon dioxide (CO_2) and water
- a diesel particulate filter (DPF) to filter out soot particles
- a catalyst for selective reduction of NO_X (SCR) using ammonia (NH_3) from decomposition of urea
- an ammonia slip catalyst (ASC) to remove excess ammonia

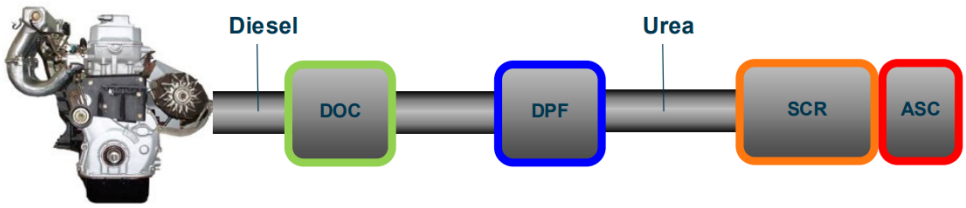

Figure 2.4 Euro 6 compliant heavy-duty diesel aftertreatment system layout (2021)

2.3.1 Diesel Oxidation Catalyst (DOC)

The DOC is made of a flow-through monolithic substrate made of ceramic or metal coated with a platinum group metal catalyst. The small parallel channels present a large contact area to the exhaust gases.

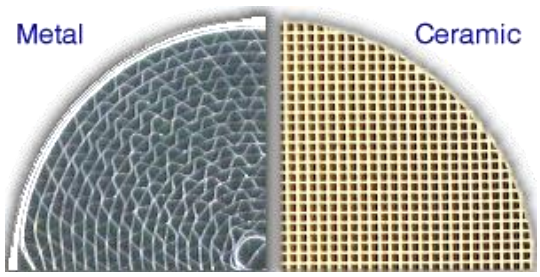

Figure 2.5 Monolithic catalyst substrates (Majewski, 2022)

Unburnt fuel (hydrocarbons) and CO are oxidized to CO_2 and water over a catalyst by using oxygen present in the exhaust. The oxidation of hydrocarbons and CO over the DOC can be described by the following reactions (Majewski, 2024a):

$$C_nH_{2m} + (n + \frac{m}{2})O_2 \rightarrow nCO_2 + mH_2O \quad (2.1)$$

$$2CO + O_2 \rightarrow 2CO_2 \quad (2.2)$$

An important secondary function of the DOC is to oxidize NO to NO_2 which is needed for passive regeneration of the DPF and can also improve low temperature performance of SCR catalysts (Majewski, 2024a):

$$2NO + O_2 \rightarrow 2NO_2 \quad (2.3)$$

The catalyst activity increases with temperature and a minimum of about 200°C is necessary for light-off. Since these oxidation reactions are exothermic, a rich exhaust mixture can heat up the DOC but this requires a high enough temperature to prevent quenching of the HC oxidation. At an inlet temperature of 260°C, the DOC outlet temperature can be raised by upto 200 K but the HC conversion is below 60%. A temperature increase of 300 K is possible with higher HC conversion but this requires inlet temperatures of above 300°C (Kumar et al., 2018).

2.3.2 Diesel Particulate Filter (DPF)

The DPF is commonly made of an extruded cordierite wall-flow monolith with precisely controlled porosity. It consists of many small parallel channels alternately plugged at each end, forcing the gas to flow through the porous walls to physically capture the solid fraction of diesel exhaust particulates including elemental carbon (soot).

An illustration of how this differs from flow-through substrates is shown in Figure 2.6.

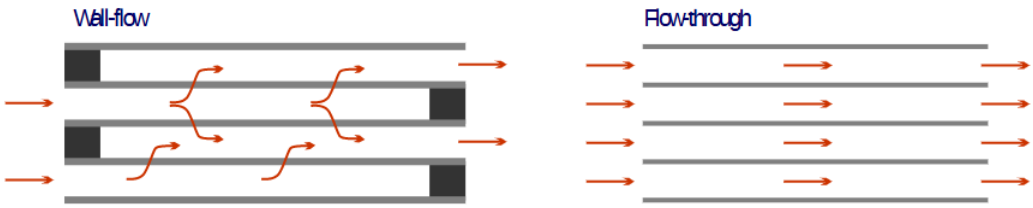

Figure 2.6 Wall-flow and flowthrough substrates: Flow pattern (Majewski, 2020)

DPFs can quickly accumulate considerable volumes of soot, causing excessively high pressure drop in the exhaust system and negatively affecting engine operation. To combat this and restore soot filtering capacity, thermal regeneration of the filter is typically employed to oxidize soot particulates at high temperatures. Two methods of regeneration commonly used are passive regeneration – continuous regeneration during engine operation, and active regeneration – increase of filter temperature by exhaust heating.

The oxidation of soot in the DPF can be described by the following reactions:

$$C + O_2 \rightarrow CO_2 \quad (2.4)$$

$$2C + O_2 \rightarrow 2CO \quad (2.5)$$

Equations (2.4) and (2.5) require temperatures above 550°C that are not usually seen in normal operation. The presence of NO_2 can reduce the oxidation temperature of soot particles to 200-300°C and enable passive regeneration of the DPF (Jiao et al., 2017) through Equation (2.6) and subsequently Equation (2.4).

$$C + NO_2 \rightarrow CO + NO \quad (2.6)$$

However, this requires an upstream oxidation catalyst and/or a catalytic coating on the DPF to increase the concentration of NO_2 in the exhaust by oxidizing NO.

2.3.3 Selective Catalytic Reduction (SCR)

Aqueous urea solution, known as diesel exhaust fluid (DEF) is injected into the exhaust stream which then evaporates and decomposes into ammonia.

$$CO(NH_2)_2 + H_2O \rightarrow 2NH_3 + CO_2 \quad (2.7)$$

The decomposition of DEF to ammonia requires a temperatures upwards of 150°C, and urea dosing can only start when this temperature has been reached. The ammonia then reacts with NO and NO_2 in the exhaust gas over a flow-through honeycomb substrate with a washcoat of catalysts that are usually made of copper-zeolite or iron-zeolite.

The catalyzed ammonia reactions with NO_X are dependent on the ratio of NO_2/NO_X in the exhaust gas and are categorized as standard, fast and slow SCR reactions:

- $\frac{NO_2}{NO_x} < 0.5$ (Standard SCR):

$$4NH_3 + 4NO + O_2 \rightarrow 4N_2 + 6H_2O \quad (2.8)$$

- $\frac{NO_2}{NO_x} = 0.5$ (Fast SCR):

$$2NH_3 + NO + NO_2 \rightarrow 2N_2 + 3H_2O \quad (2.9)$$

- $\frac{NO_2}{NO_x} > 0.5$ (Slow SCR):

$$8NH_3 + 6NO_2 \rightarrow 7N_2 + 12H_2O \quad (2.10)$$

At NO_2/NO_X ratios higher than 0.5, the excess NO_2 also promotes the formation of byproducts such as N_2O. The best target ratio for NO_X reduction is then 50% for the fastest NO_X reduction without unwanted production of N_2O. This is especially true for temperatures below 300°C.

The SCR process requires precise control of ammonia injection. Too little results in insufficient NO_X conversion and too much results in release of unreacted ammonia to the atmosphere. The stoichiometric ratio of ammonia to NO_X in the standard and fast SCR reactions is 1. The molar ratio of ammonia to NO_X is called the ammonia to NO_X ratio (ANR). To ensure sufficient conversion, ANR greater than stoichiometric 1 are often used but this can cause ammonia slip.

The NO_X conversion efficiency for the catalyst is temperature dependent. The light-off temperature for 50% conversion (T_{50}) for typical commercial SCR catalysts is about 200°C. However, if too high temperatures are reached, the catalyst can lose selectivity, unfavorable reactions that create pollutants can be promoted, and thermal degradation of the catalyst can occur.

The SCR washcoat can store substantial amounts of NH_3 especially at low temperatures. This is then released at higher temperatures which is particularly important in transient engine operation.

2.3.4 Ammonia Slip Catalyst (ASC)

The use of ANR > 1 and transient operation often result in ammonia slip past the SCR due to some channels of the substrate getting more ammonia than required for the reaction, which is then oxidized to N_2 and H_2O over the ASC.

The ASC is a flow-through cordierite substrate with a washcoat of catalysts placed downstream of the SCR. To improve selectivity for N_2 and reduce formation of N_2O and NO_X, ASCs today commonly combine a dual oxidation-SCR function.
On the lower oxidation layer containing platinum group metals over an oxide like alumina the following reactions take place:

$$4NH_3 + 3O_2 \rightarrow 2N_2 + 6H_2O \quad (2.10)$$

$$4NH_3 + 5O_2 \rightarrow 4NO + 6H_2O \quad (2.11)$$

$$2NH_3 + 2O_2 \rightarrow 2N_2O + 3H_2O \quad (2.12)$$

$$NO + \frac{1}{2}O_2 \rightarrow NO_2 \quad (2.13)$$

On the top layer with SCR coating where ammonia is stored, reactions (2.8), (2.9) and (2.10) take place to reduce the NO_X produced from the lower layer as well as some non-reduced NO_X in the exhaust gas.

2.4 Close-coupled SCR

Diesel engines generally have lower exhaust temperatures compared to gasoline engines, which becomes particularly pronounced during cold starts and low-load operation. Hence, high levels of NO_X, CO and HC are expelled from the tailpipe during warm-up phases from cold start and during low-load operation when the catalysts are below light-off temperature. The first 350s of a cold start cycle can contribute more than 50% of the total tailpipe NO_X emissions of a test cycle, see Figure 2.7 (Kim et al., 2012).

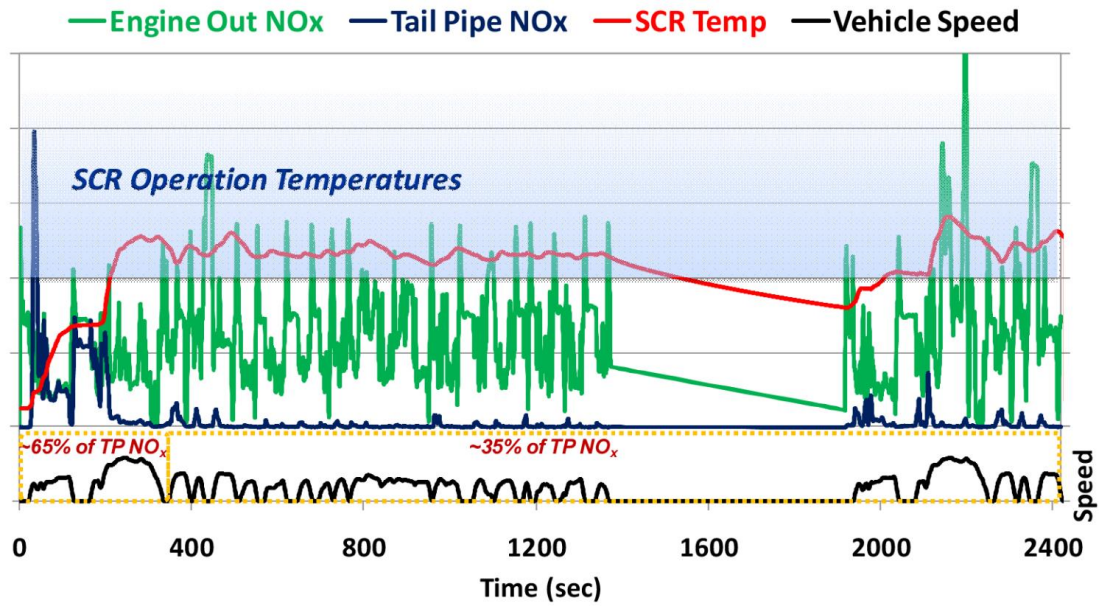

Figure 2.7 SCR temperature and NO_X during the cold FTP-75 cycle

In conventional exhaust systems, the aftertreatment components are heated by the hot exhaust gas from the engine. This means that there is a significant thermal mass to heat up, and the downstream components like the SCR heat up slower than the upstream components.

A close-coupled SCR (ccSCR) placed close to the engine exhaust can be heated faster, and the NO_X conversion can start earlier. Two possible ccSCR installation layouts are shown in Figure 2.8.

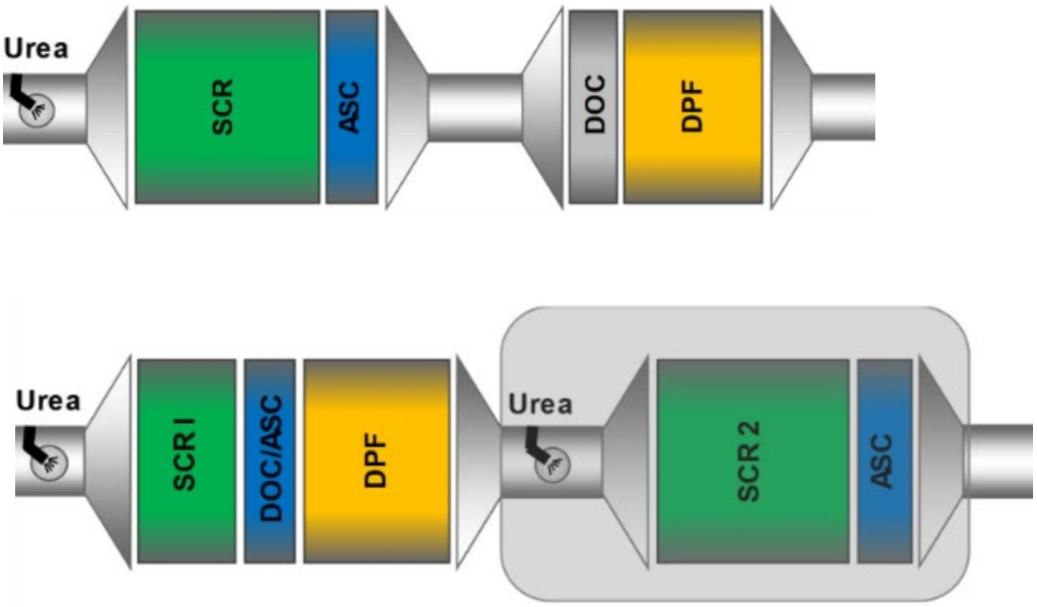

Figure 2.8 Two possible ccSCR layouts (The Danish Environmental Protection Agency, 2021)

Th use of a ccSCR element has been shown to reduce NO_X emissions by 10-25% in cold start cycles, and 40-70% in warm start cycles by shortening the time to reach 180°C at the ccSCR from about 470s to about 70s (The Danish Environmental Protection Agency, 2021). Tests on a Euro 6 long-haul truck equipped with a close coupled DOC and SCR have demonstrated significantly faster light-off time for the SCR catalyst and ultra-low NO_X emissions in various drive cycles and ambient conditions (Mendoza Villafuerte et al., 2021).

2.5 Exhaust heating strategies

To assist with faster heat-up of the exhaust in cold-start and low-load conditions, a combination of engine-based heating strategies are commonly used.
Some of these are:

- Intake throttling
  By restricting the airflow into the intake manifold, pumping work is increased and the air -fuel mixture is enriched.

- Exhaust throttling
  By restricting the exhaust flow to increase backpressure, pumping work is increased and the air-fuel mixture is enriched.

- Late injection
  Injecting fuel late in the combustion cycle results in inefficient combustion. A further strategy is post-injection to have unburned fuel that can oxidize in the exhaust directly converting fuel energy into heat.

- Increased idle speed
  A higher idle speed involves injecting more fuel into the cylinders which generates additional heat in the engine. The increased combustion leads to a larger amount of exhaust gases from the engine which heats up the catalysts downstream faster.

- Variable valve timing (VVT)
  Late intake valve opening (IVO) reduces the amount of fresh air entering the cylinders, leading to a richer air-fuel mixture. Early exhaust valve opening (EVO) reduces expansion in the cylinders and increases exhaust gas temperature. Both late IVO and early EVO reduce the effective expansion ratio of the cycle and results in less work extraction. VVT can be implemented with cam phasers, individually activated valves and multiple cam lobes.

- Cylinder deactivation (CDA)
  By selectively deactivating cylinders, the load on the remaining active cylinders increases resulting in higher exhaust temperatures.

Although additional heating devices are not needed, most of these techniques work by decreasing the efficiency of the engine or increasing fuel injection resulting in a fuel consumption penalty. In addition, poor combustion sometimes results in higher emissions, typically unburned hydrocarbons and carbon monoxide.

During warm-up, the bulk of the heat energy released from combustion is used to warm up the engine mass. Only 11-16% of the fuel used is effectively converted into raising exhaust gas temperature (Jarrier et al., 2000; Romero et al., 2014). This means that for any additional fuel injected for exhaust heating, only about 11-16% would have resulted in conversion of energy to the exhaust. Further, some of this energy is lost to heating up exhaust system components upstream of the catalysts and to the ambient air.

An external heat source to heat up the catalysts independent of the engine is a potential solution. Common approaches to delivering external heat to the catalysts are:

- Fuel burners
  Fuel is injected and burned in the exhaust upstream of the catalysts. This setup is independent of exhaust temperature and allows fast heatup. However, it requires more hardware for dosing, ignition, air supply and control making it a complicated solution.

- HC dosing
  Fuel is added to the exhaust gas through very late injection in the engine or using a dedicated injector in the exhaust system. This fuel mixture is then oxidized over a DOC to generate heat. This solution is simpler but requires a temperature of atleast 200°C to be able to start oxidation at the DOC.

- Electric heating
  An electric heating element can be used to generate heat in the exhaust system. This solution can deliver fast, targeted heating and can be controlled independent of engine operating conditions.

2.6 Electric heaters

Electric heaters work by converting electrical energy into thermal energy through the Joule effect by passing an electric current through a resistive heating element. The power consumed by the heater can be described by the following equation:

$$P = \frac{U^2}{R} \tag{2.14}$$

Here, *R* is the resistance, and *U* is the voltage across the heating element.

Electric catalyst heating can be implemented in different ways:

- Catalyst substrate heating where electric current is passed through the substrate to heat it
- Catalyst skin heating where an electric heater is wrapped around a catalyst
- Upstream exhaust gas heating

Direct heating of the catalyst is faster and more energy efficient as the energy is targeted at the catalyst mass. However, there are limitations. Catalyst skin heating has been found to be ineffective at transferring heat to the core of the catalyst. Catalyst substrate heating distributes heat evenly across the volume but the exhaust flow tends to transfer this heat towards the outlet resulting in lower temperatures at the catalyst inlet (Hamedi et al., 2021).

Additionally, for SCR systems to work effectively the exhaust gas temperature needs to be high enough for evaporation and hydrolysis of DEF to ammonia. If the exhaust gas temperature is too low, the absence of gaseous ammonia will prevent NO_X conversion even if the SCR catalyst itself is directly heated. Heating the exhaust gas upstream of the SCR can raise the overall gas temperature to a level that allows for efficient DEF injection and subsequent NO_X reduction (Culbertson et al., 2018). Heating the exhaust gas upstream can also help in evaporating moisture in the exhaust gas which can hinder the catalyst's effectiveness and delay its activation (Culbertson et al., 2015).

The increase in temperature of the exhaust gas can be described by the following equation:

$$T_{out} - T_{in} = \frac{\eta_h . P}{\dot{m} . C_p} \tag{2.15}$$

Here, P is the electrical power applied to the heater, η_h is the thermal efficiency of the heater, $\dot{m}$ is the exhaust mass flow, C_p is the specific heat capacity of the exhaust fluid, and T_{out} and T_{in} are the heater outlet and inlet temperatures. The thermal efficiency of the heater depends on heat losses to the ambient environment. Colder ambient temperatures or larger air flow on the exterior of the heater decrease thermal efficiency. A typical value for η_h is 0.9 (Culbertson et al., 2016).

A smaller diameter heater results in a higher velocity flow over the heating elements which can transfer heat more effectively. However, this also increases exhaust backpressure and increases fuel consumption.

The most common type of heater is a metal honeycomb design made of ferrochrome aluminum. The heating material is formed into flat or corrugated sheets and rolled into and S-shape or spiral form. The heating material is supported by an insulating material, typically ceramic, to fasten it to the support body. The interior space is divided into a consistent through-aperture structure, giving the appearance of a honeycomb (Li et al., 2024).

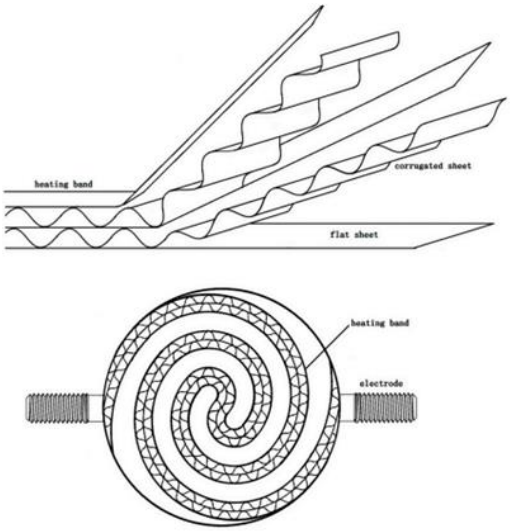

Figure 2.9 Structure of a rolled electric heater (Li et al., 2024)

A different design developed by HJS Emission Technology GmbH shown in Figure 2.10 uses a heating band bent to form a bow-shaped structure held by ceramic inserts on a support frame. This design claims a low exhaust backpressure compared to the honeycomb design showing high potential for fuel savings and emission efficiency (Lindemann et al., 2022). Due to the support frame and relatively large width and thickness of the heating band, this type of heater is likely more sturdy than honeycomb heaters (Li et al., 2024).

Figure 2.10 HJS heater band (Lindemann et al., 2022)

The power for an electric heater will ideally be supplied by an alternator when the engine is running, or by a battery when the engine is off. Using the alternator increases engine load results in higher engine-out exhaust gas temperatures and can lead to better specific fuel consumption.

Even with low power heating designs using the 12 V DC electrical system and alternators on passenger cars in the 1990s, significant reductions were seen in cold-start HC emissions (Kubsh & Brunson, 1996; Küper et al., 1994). Today, a 24 V electrical system is common on heavy-duty vehicles, with hybrid vehicles featuring 350 V systems for the electric powertrain. Higher voltage electrical systems make it easier to utilize higher power heaters without much adaptation for high currents.

2.7 Previous relevant work

Studies have shown significant reduction in light-off time for SCR catalysts when using an electric heater in diesel engine installations.

1D simulations of a 12.8 liter Euro 6 engine with a 10 kW heater on a cold WHTC showed an SCR inlet temperature of 200°C under 50 seconds even without considering the heat from the additional engine load. Tests of a 40 ton Euro 6 truck equipped with twin dosing and an upstream electric heater in an urban delivery cycle showed a 50% reduction in NO_X emissions (Lindemann et al., 2022).

Tests on a 6.7 liter 230 hp diesel-electric hybrid with a heater placed between the DOC+DPF and SCR units showed a reduction of more than 6 minutes on a Federal Test Procedure (FTP) cold cycle when using a 12 kW heater, and more than 8 minutes when using a 30kW heater (Culbertson et al., 2015). Tests on a 6.7 liter 230 hp diesel engine with a heater placed before the DOC+DPF and SCR units showed that 4kW was sufficient to maintain a temperature of 275°C at the DOC inlet in a city bus cycle This cycle consists of frequent stops and without the heater the DOC inlet temperature is around 200°C. Results from this test also show that when powering the heater using the alternator, the additional engine load increases engine outlet temperature. This additional load increases engine out NO_X emissions, but the tailpipe NO_X emissions when using a heater is much lower. When powering the heater using the alternator, the maximum required heat flow from the heater is reduced, and the engine operates at a higher efficiency because of the increase in load. This potentially translates to fuel savings (Culbertson et al., 2018).

When installed together with close-coupled catalysts and dual dosing, using an electric heater has been shown to accelerate the time to catalyst light-off even more. Tests on a Euro 6 truck performing urban delivery cycles showed that ccSCR temperatures can be increased by 50-100°C during cold-start using a 12 kW heater compared to a system without an electric heater. NO_X slippage was avoided during long stops by preserving the temperature in the catalysts (Mendoza Villafuerte et al., 2022).

Using an electric heater together with CDA have shown good results with lower heater power. Tests were performed on a 500 hp 15 liter diesel engine equipped with CDA and a 10kW heater placed upstream of a ccSCR unit. A maximum power level of 2.4kW was found to show an optimal trade-off between NO_X and CO_2 emissions. Compared to using only CDA, using the electric heater showed a reduction of 40 % in

NO_X emissions on a cold FTP test cycle while also saving 1.6% CO_2. On a hot FTP cycle, there was no reduction of NO_X but CO_2 emissions reduced by 1.9% (Zavala et al., 2022).

3 Method

The exhaust aftertreatment system used by Scania on its Euro 6 compatible vehicles includes dual SCR dosing points with a ccSCR unit (referred to as SCR1) for emission reduction at cold starts and low load operation.

Installing an electric heater upstream of the ccSCR unit is expected to reduce the time to catalyst light-off and reduce NO_X emissions at cold start, and to keep the catalyst warm during low-load operation. A 10kW electric heater similar to the one shown in Figure 2.10 was used for this evaluation. Tests in an air flow rig and engine test cell were complimented with 1D simulations to evaluate the performance of a 10 kW heater in NO_X reduction and energy consumption for a cold WHTC, low load cycle and long idle.

3.1 Aftertreatment system

The tests in this evaluation were performed with a Euro 6 silencer and a 10 kW electric heater installed upstream of the silencer with a diffuser cone.

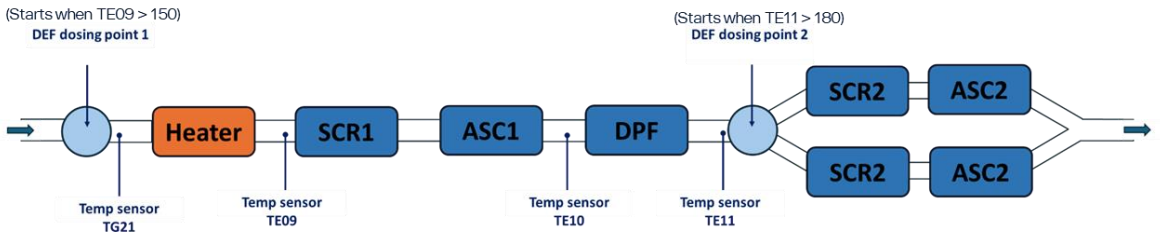

Figure 3.1 Layout of aftertreatment system with heater

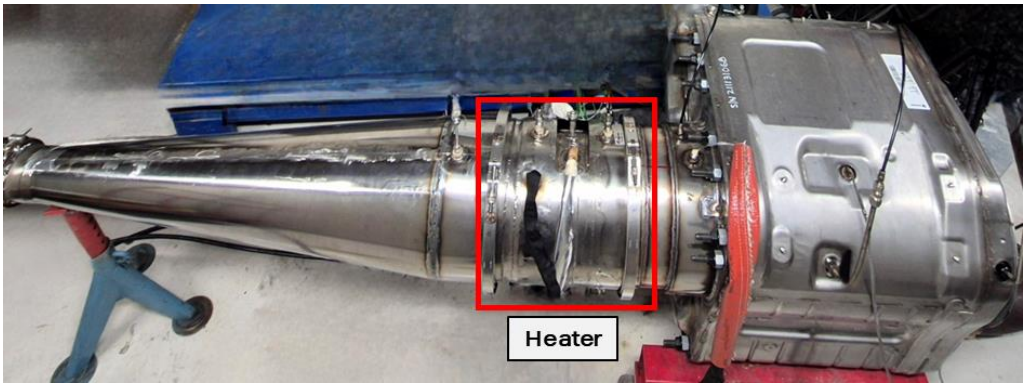

Figure 3.2 Silencer with heater and diffuser cone

3.1.1 Silencer

This silencer contains all the components downstream of the heater in Figure 3.1. The first DEF dosing point is located after the turbocharger outlet. The silencer was modified to have a new inlet position to allow flow from the heater outlet to enter SCR1 directly without a reduction in diameter.

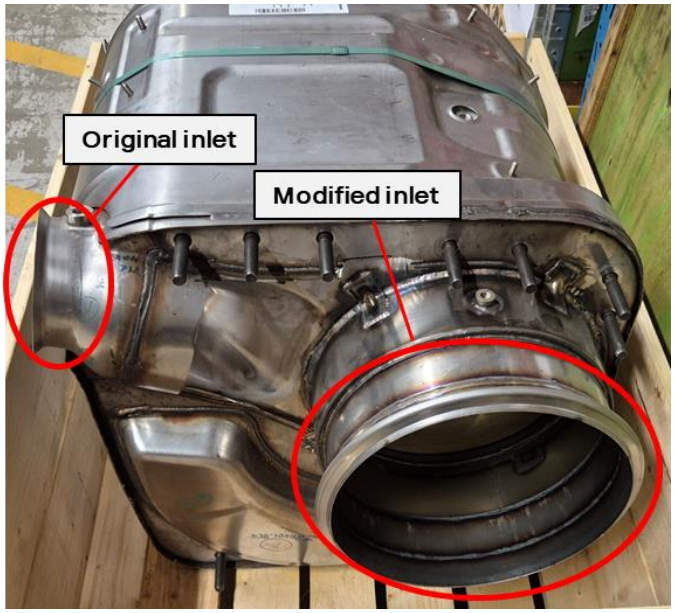

Figure 3.3 Original and modified silencer inlets

3.1.2 Heater

A 10.5-inch diameter prototype heater from HJS Emission Technology GmbH similar to the design in *(Lindemann et al., 2022)* was used for these tests. This heater is rated for 10 kW at 48 V DC and promises a low pressure drop less than 1 mbar @ 1000 kg/h due to the large open frontal area. For installation with the silencer, a stainless steel casing was built around the heater. Because of the significantly larger diameter (267 mm) of the heater than the standard exhaust outlet (120 mm), a diffuser cone was installed before the heater.

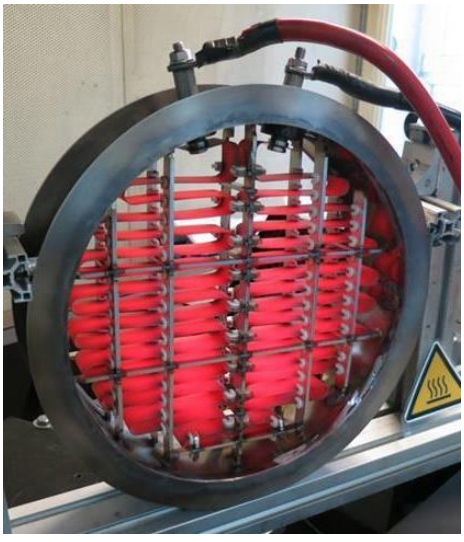

Figure 3.4 Heater during tests at supplier

The heating band works as an ohmic resistor and has a positive temperature coefficient (PTC) of approximately 120 ppm/K. This means resistance increases with temperature, limiting the current flowing through it and stabilizing at some point. The resistance through the band was measured close to 0.235 Ω at 22°C. Using the PTC

value, this gives us the maximum power that can be drawn by the heater as the temperature of the band increases.

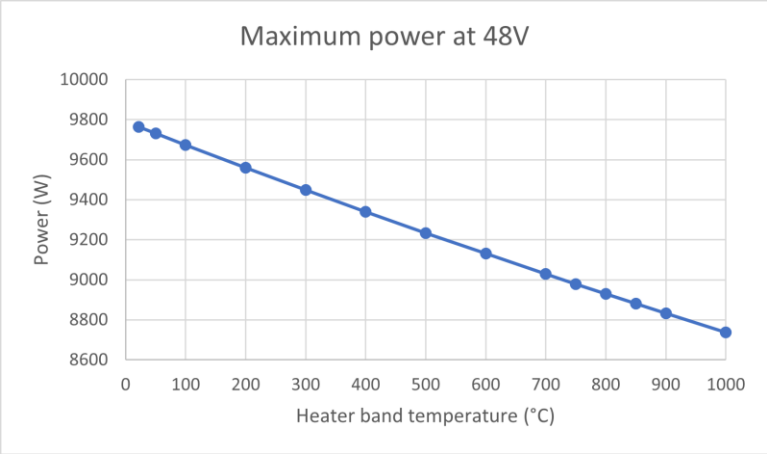

Figure 3.5 Maximum heater power vs temperature

Maximum allowed power was limited for lower mass flow rates and higher exhaust gas temperatures to prevent damage to the heater, using data from the supplier.

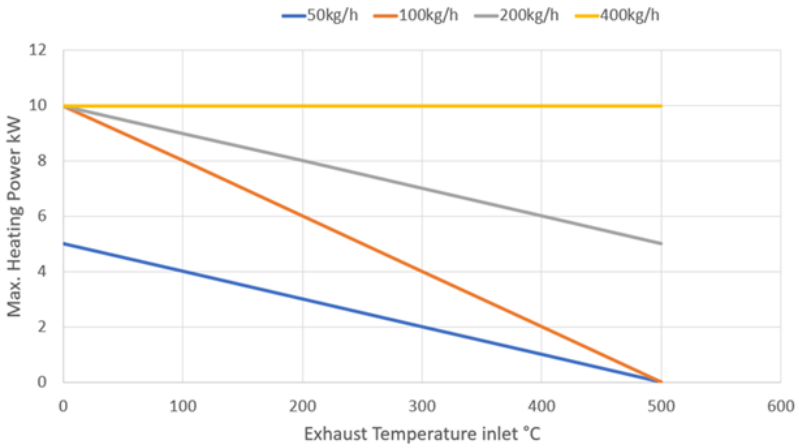

Figure 3.6 Maximum allowed heater power vs exhaust gas temperature

Power to the heater was supplied by an adjustable power supply unit. Voltage and allowed current for requested heater power values were calculated by scaling between 0 and the maximum of 48 V and 208 A for 10 kW. Voltage at the heater terminals was constantly measured by the power supply unit to compensate for any voltage drops in the power cables to the heater.

In the flow rig test, power requests were manually sent to the power supply unit using a PC and USB interface. For the engine test cycles with varying mass flow and exhaust temperature, power requests to the power supply unit were sent by the test cell control system by using a lookup table to interpolate maximum allowed power for the current mass flow and exhaust temperature values.

3.1.3 Sensors

There are three standard temperature sensors used by the engine management system for estimating temperatures inside the silencer:

- TE09: Gas temperature sensor at silencer inlet. Repositioned to the modified SCR1 inlet.
- TE10: Gas temperature sensor before DPF.
- TE11: Gas temperature sensor before dosing point 2.

Additional sensors used for the flow rig and engine tests are mentioned in sections 3.2.1 and 3.3.1.

3.2 Flow test

Steady state tests were performed in an air flow rig to evaluate the performance of the heater in this installation. The test rig is capable of flowrates between 200 and 2400 kg/h upto 550°C. However, there are limitations on what temperature can be maintained at a specific flowrate because this rig is best suited for flows above 700 kg/h and 120°C.

3.2.1 Test setup

Although not ideal, due to space constraints, the heater and silencer installation was made with a 90° bend before the diffuser inlet.

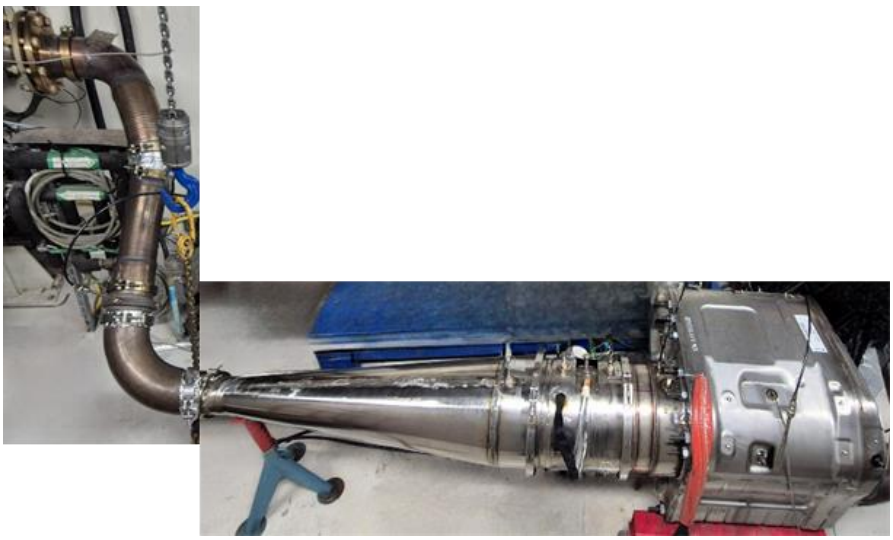

Figure 3.7 Silencer and heater installation in air flow rig

Additional K-type wire thermocouples of 0.5 mm diameter were used to capture radial temperature distribution at select points in the exhaust path.

A grid of 11 thermocouples was installed 70 mm after the heater band. These were positioned in pairs such that each pair consisted of a ‘hot’ sensor (orange) directly facing the heater band and a ‘cold’ sensor (blue) in the gap between adjacent band

sections as seen in Figure 3.8. A simpler grid with three thermocouples was installed 70 mm before the heater band to measure temperature of air flowing into the heater.

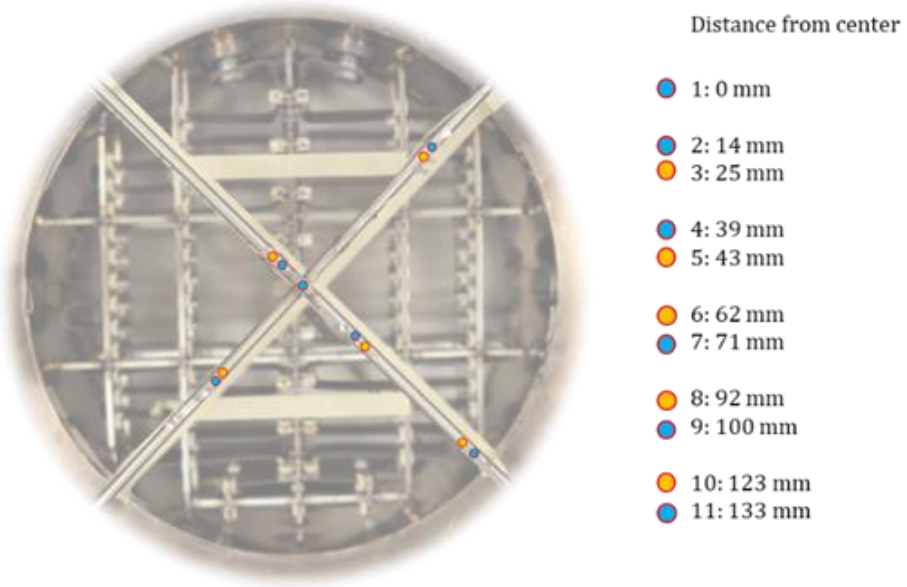

Figure 3.8 Thermocouple grid after heater

Thermocouples were also installed to capture temperature distribution at SCR1 inlet and inside the brick as seen in Figure 3.9:

- TG_SCR1_x: Gas temperature at SCR1 inlet
  Thermocouples placed just above the surface of the SCR1 brick.

- TS_SCR1_x: Solid temperature at mid-depth of SCR1
  Thermocouples placed inside SCR1 at mid-depth.

The naming convention for radial position of the sensors are as follows:
1, 2, 3 correspond to radial distance from center. 1: 0 mm, 2 : ~70 mm, 3 : ~140 mm

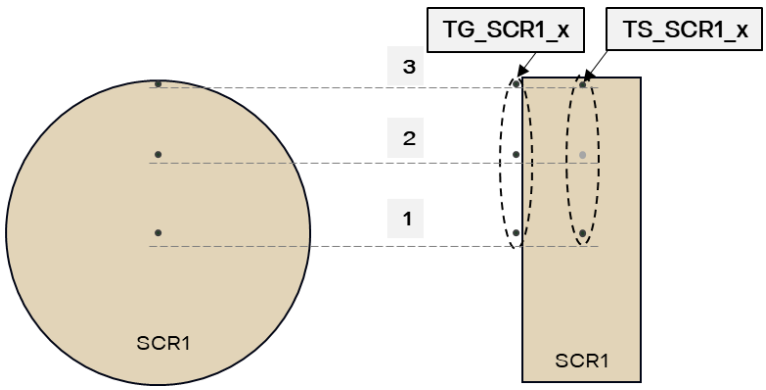

Figure 3.9 SCR1 thermocouples in flow rig test

Pitot tubes were also installed to measure total pressure before and after the heater.

3.2.2 Results

At temperature requests below 120°C, flow temperature cannot be controlled and depends on inlet ambient air temperature and heat added by the fan motor. Above 120°C, higher flowrates are required to maintain stable flow and inlet temperature. However, a few test cases in the uncontrollable areas were run by manually toggling setpoints for the flow and temperature controller back and forth in the rig.

During the test period, the lowest stable inlet temperature was ~30°C at 200 kg/h. A majority of tests were performed at this point due to the limitations of the rig and the primary intended use case of the electric heater being low flowrates (100 to 300 kg/h) and cold starts (30°C or lower).

A clear stratification of hot and cold streams of air corresponding to the ‘hot’ and ‘cold’ temperature sensors was observed after the heater as seen in Figure 3.10. However, the radial temperature profile did not follow a clear trend. Note that only the blue and orange points are actual measurement locations.

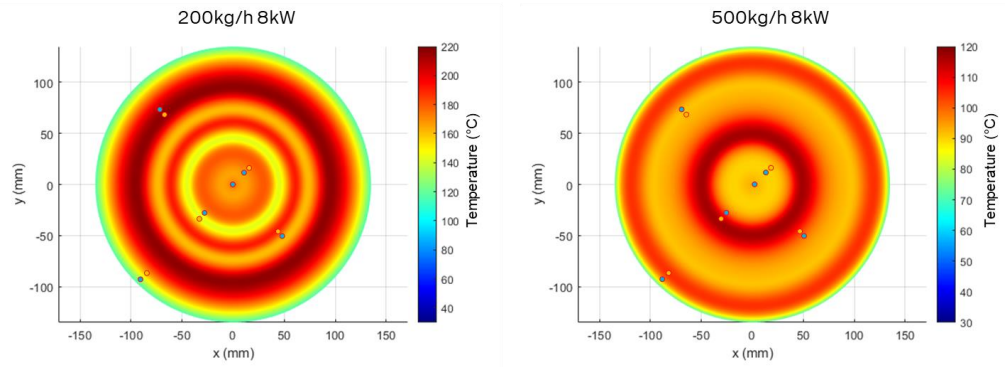

Figure 3.10 Temperature distribution 70 mm downstream of heater

The maximum observed temperature in the center of the SCR1 block for varying flowrates and heater powers at steady state are shown in Figure 3.11. This is for an inlet temperature of 30°C but a few test runs for 50 and 110°C showed very similar increases in temperature.

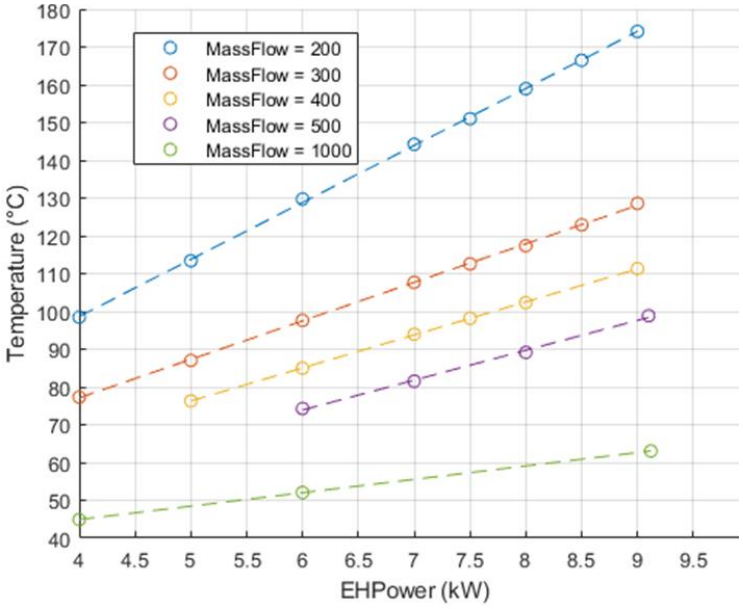

Figure 3.11 Maximum temperature at TS_SCR1_1

If the exhaust gas was evenly heated, the temperature increase could be estimated using equation (2.15). Comparing this ideal temperature increase to measured values, we can see increasing heat losses at higher heater powers for most of the flow rates which is likely due to increased heat transfer through the walls as seen in Figure 3.12. However, negative values are seen for the higher flow rates. This is because of uneven flow distribution through the heater, which results in uneven heating and hot regions at the measurement point in the SCR1 block.

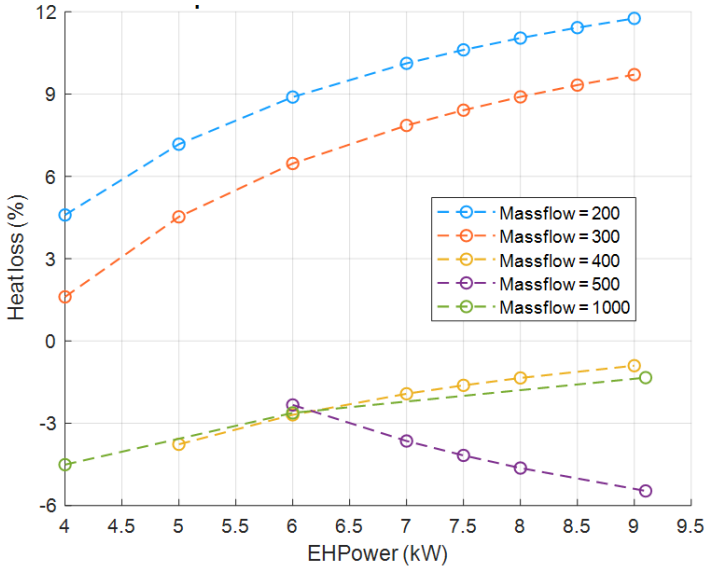

Figure 3.12 Heat losses at TS_SCR1_1

Figure 3.13 shows time taken for a 50 K increase in SCR1 solid temperature for different flow rates and heater powers with 30°C inlet air temperature. Similarly, Figure 3.14 shows the rate of increase of SCR1 solid temperature for the same points.

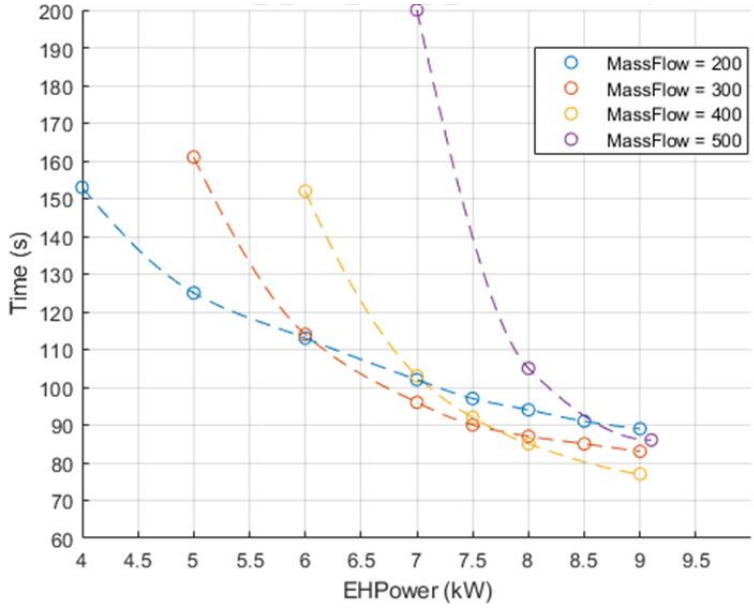

Figure 3.13 Time for 50 K increase at TS_SCR1_1

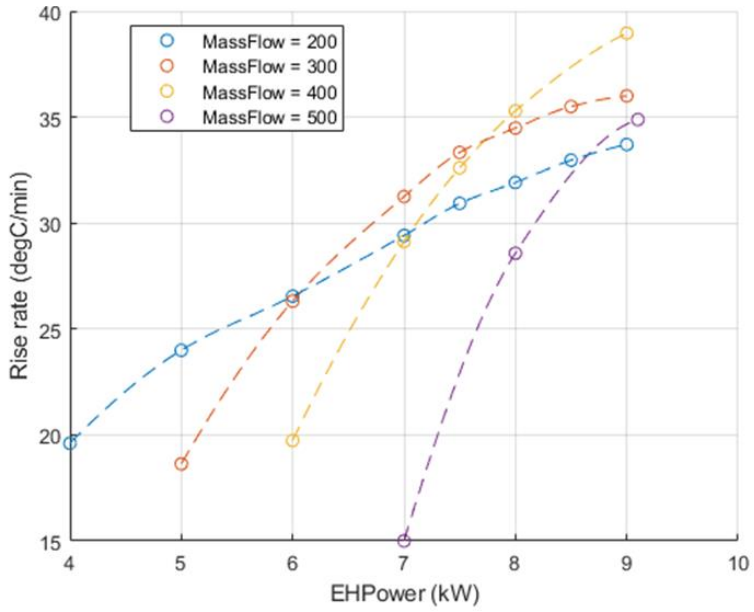

Figure 3.14 Rise rate for 50 K increase at TS_SCR1_1

Higher heater power equals faster heatup of the SCR1 brick as expected. But over roughly 7.5 kW, the gains from increasing heater power are reduced. For lower heater powers, the SCR1 brick heats up faster at lower flowrates because air temperature from the heater outlet is higher as seen in Figure 3.11. But beyond roughly 7 kW, higher flow rates heat up the SCR1 brick faster because of increased rate of heat transfer from the heated air to the SCR1 brick. The trend in the 500 kg/h case is different from the others and this is attributed to worse flow distribution at higher flows as seen in Figure 3.12.

Comparing the distribution of gas temperature entering the SCR1 block and solid temperature inside the block for a low and high flow rate case at the same heater power as seen in Figure 3.15 and Figure 3.16, the maldistribution is clearer.

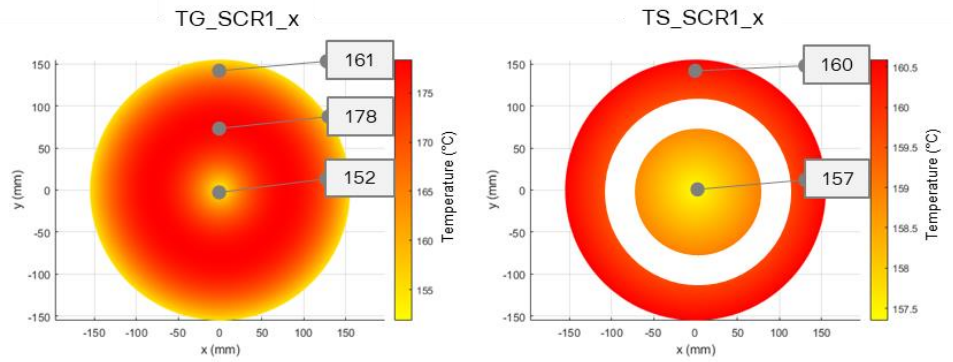

Figure 3.15 SCR1 temperature distribution at 200 kg/h and 8 kW

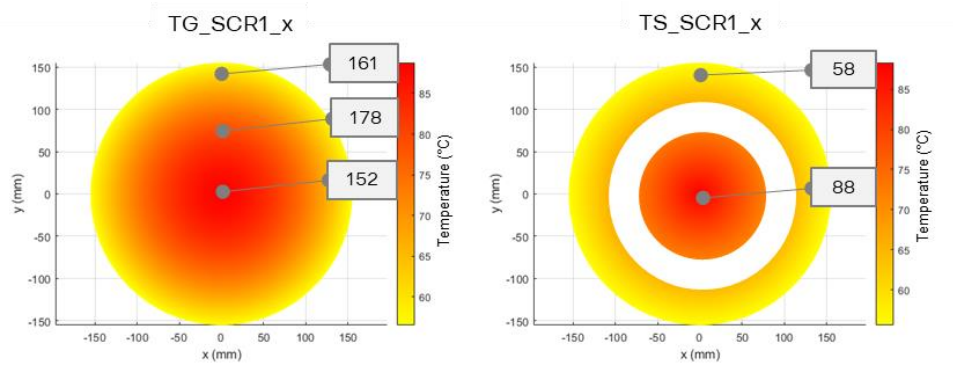

Figure 3.16 SCR1 temperature distribution at 500 kg/h and 8 kW

In the 200 kg/h case, the center is coldest for both gas and solid. Ideally, the center is expected to be warmest and colder towards the outside due to heat losses to the walls of the inlet pipe and SCR1 block casing. In the 500 kg/h case, the center is the warmest but with higher temperature than expected. Since only three measurement points were available for both gas and solid, it is likely that this is not be an accurate representation of the radial temperature profiles across the plane, and there may have been other hot or cold spots.

To help understand the flow behavior in this setup, a simple simulation study was performed by a colleague for the 200 and 500 kg/h cases.

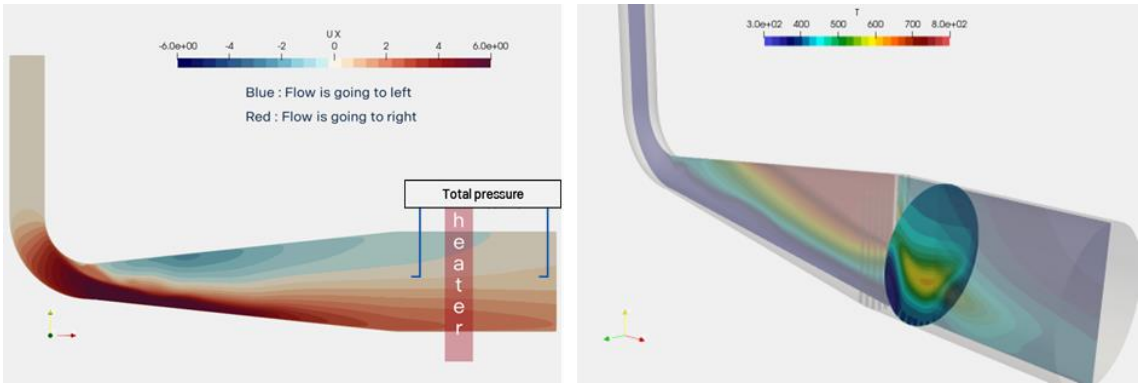

Figure 3.17 Axial velocity and temperature distributions at 200 kg/h

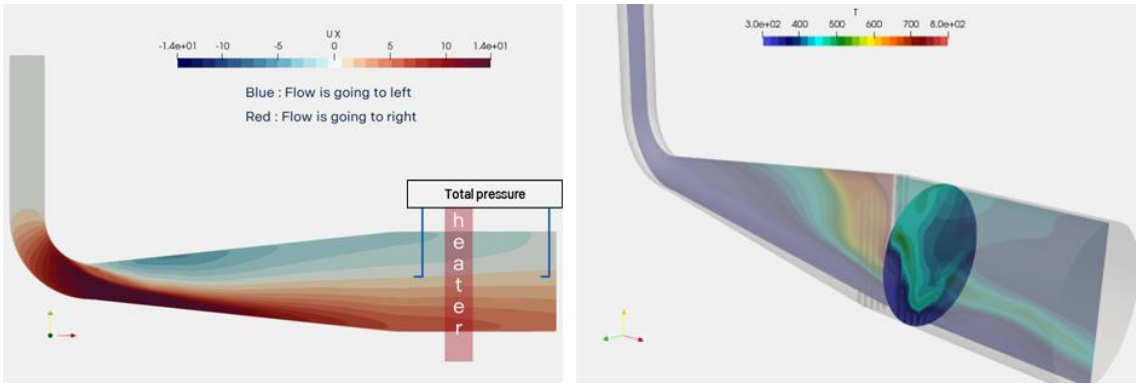

Figure 3.18 Axial velocity and temperature distributions at 500 kg/h

As seen in Figure 3.17 and Figure 3.18, in both cases, flow separates at the bend before the diffuser inlet, expanding through the diffuser and creates a large recirculation zone before the heater. This leads to stagnant and even reverse flow through a large area of the heater face resulting in uneven gas temperature at the SCR1 inlet. In the 500 kg/h case, the hotspots at the SCR1 inlet are even more localized, This explains the higher than expected SCR1 solid temperature mentioned earlier.

Total pressure measurements after the heater were higher than before the heater, even with different pressure sensor types and ranges. This unexpected behavior can be explained by the upstream pitot tube's position in the recirculation zone as shown in Figure 3.17.

In an attempt to straighten and improve the flow, an unplugged core cutout from a DPF block was used at the diffuser inlet. This mildly improved the distribution for the 200 kg/h case making the center the warmest but it made the 500 kg/h case worse. Another attempt to minimize the flow separation due to the bend was made by installing a 700 mm long straight section before the diffuser and keeping the DPF core installed. This did not improve the temperature distribution significantly either.

To reduce the flow maldistribution, a large pressure drop is required. Another solution is to use flow guiding devices like vanes to direct the flow. Neither of these options were possible to test at the time.

The gas temperature measured at TE11 (after DPF and before dosing point 2) was almost 20 K higher than at TE10 (before DPF) for the 500 kg/h case. A lower temperature at TE10 is sometimes observed because of the sensor position but this difference was much higher than expected. This pointed to a significant temperature maldistribution continuing even after the SCR1 and ASC1 blocks. This likely meant that the pressure drop due to the SCR1, ASC and DPF blocks were likely insufficient to balance the flow.

The maximum power that could be drawn from the heater in all test cases was 9 kW at 48V. This is likely because of too high temperatures at some parts of the heater band due to poor air flow, which increases the resistance locally and limiting current through the entire circuit.

The heater band reaches around 800°C when energized. At this temperature, there is significant transfer of heat by radiation to the components exposed to it. This also affects the temperature sensors before and after the heater. Ideally, only heat transfer from the gas flowing around the sensors is desired for measuring gas temperature. The contribution of radiative heat transfer on the sensors is difficult to calculate as it requires knowing the temperature of the heater band, view factor, emissivity values for both the heater band and sensor, and heat transfer to the gas around the sensors.

A common rule in metrology is that the radiative error depends on the square root of the sensor diameter and inversely on the square root of the air speed past the sensor (de Podesta et al., 2018). To minimize radiative error, a common approach is to use very small sensors, so the smallest available (0.5 mm diameter) wire thermocouples were used.

An attempt was made to see if having two similar sensors at different distances from the heater band would show a relationship between the measured temperature and distance from the band. A larger distance equates to a smaller solid cone angle of the heater band exposed to the sensor. As shown in Figure 3.19, sensor TG_EH_UT_1 was at a distance 70 mm from the heater band and sensor TG_cone_out was placed at 140 mm from the band. The heater was energized with 8 kW of power with no air flow for 30 seconds to observe how the temperature increases in the two sensors.

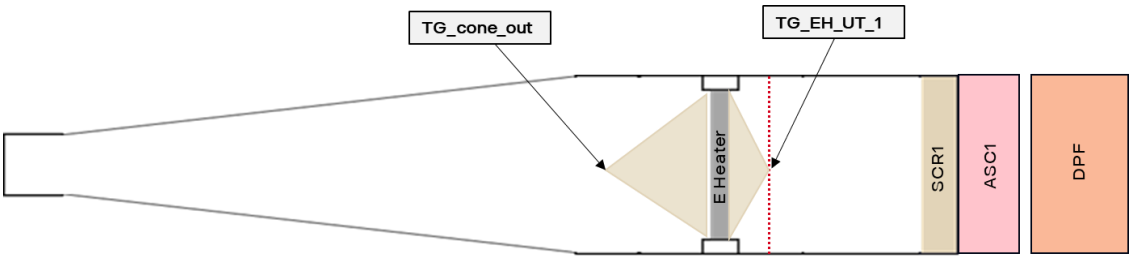

Figure 3.19 Position of thermocouples for testing radiative error

Interestingly, as seen in Figure 3.20, the sensor further away from the heater band heated up faster and to a higher temperature than the one closer to the band. An explanation for this is that the inside surfaces of the heater shell, pipe and the diffuser cone are made of stainless steel and reflective, resulting in a complex ‘scene’ with reflections bouncing off several surfaces at various angles and causing some areas to receive high incident radiation.

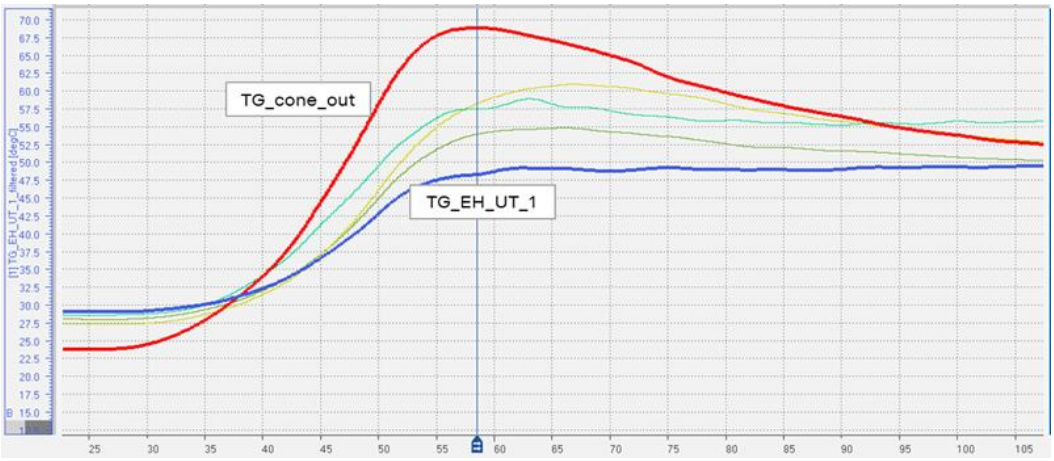

Figure 3.20 Temperature rise at thermocouples for testing radiative error

Although there is a radiative error in the measurements made by the sensors exposed to the heater band, this was negligible for sensors close to SCR1 with air flow. The difference between a sensor measuring SCR1 inlet gas temperature and one measuring SCR1 solid temperature at the same radial distance at steady state was found to be less than 3 K.

3.3 Engine test

Tests were performed using the same heater and silencer setup with a 13 liter 380 hp turbocharged diesel engine to evaluate the performance of the heater in transient cycles. The engine was coupled to a dynamometer to simulate engine load in a vehicle, and exhaust gas composition was measured using an FTIR (Fourier Transform Infrared Spectroscopy) gas analyzer. All tests were performed at cell ambient temperature 25°C and standard atmospheric pressure.

Between tests, a conditioning run at high load and no urea dosing was performed to remove soot, NO_X and NH_3 storage in the silencer. This was followed by forced cooling by motoring the engine with lowered intake and cell temperature until all the temperature sensors in the silencer showed between 20-30°C and engine oil temperature was below 50°C.

In preliminary runs while setting up the test, it was found that the exhaust gas temperature drops around 70 K between the turbocharger outlet and SCR1 inlet. This was attributed to heat losses due to the large surface area of the diffuser and the diffuser was insulated with a thick ceramic wool sheet normally used to insulate engine compartments. This reduced the heat losses but there was still almost a 60 K drop at flow rates of 250 kg/h. At higher flow rates, this drop was significantly lower.

Normally, a combination of engine-based exhaust heating techniques using an exhaust brake, cam phasing and injection timing is employed for fast heating of the aftertreatment system. The extent of engine-based exhaust heating techniques used depends on temperatures in the aftertreatment system and is categorized into two main modes:

- Thermal management (TM): Used for fast heating of the aftertreatment system using engine-based exhaust heating techniques, when temperatures in the silencer are less

than 240°C. In this mode, the engine puts out low levels of NO_X but at the cost of higher fuel consumption and soot output.
- Fuel consumption optimized (FC): When temperatures in the silencer are higher than 240°C, thermal management is not used. In this mode, fuel consumption and soot are lower, but engine-out NO_X is about three times higher than in mode 44.

There are several other modes between these two extremes but these two are considered in this evaluation. In normal operation, the engine management system (EMS) decides which emission mode to use and is referred to as mode-free operation. Tests were also performed by forcing the EMS to operate only in TM or FC modes to compare extremes.

Figure 3.21 Silencer and heater installation in engine test rig

The first urea dosing point in this installation is after the turbocharger and is only allowed to start dosing when silencer inlet temperature is above 150°C to prevent urea deposits. The second dosing point is inside the silencer after the DPF, and is allowed to start dosing when the exhaust temperature there is above 180°C. The amount of urea dosed is based on a target NH_3-NO_X ratio (ANR) of 0.4 at the first dosing point and 1.1 at the second. This is a rough approximation because the actual dosing amounts at any time vary significantly due to adaptations for urea crystallization, injector characteristics, urea mixing and SCR efficiency.

3.3.1 Test setup

In the previous test, temperature maldistribution before and inside SCR1 was observed but due to the limited number of measurement points, it was not known if the rest of the radial profile looked similar to the measured points. For this test, more thermocouples were installed to obtain a fuller picture. Thermocouples were also installed before the DPF to measure the temperature distribution of the gas entering the DPF.

- TG_SCR1_x: Gas temperature at SCR1 inlet
  Thermocouples placed just above the surface of the SCR1 brick.

- TS_SCR1_x: Solid temperature at mid-depth of SCR1
  Thermocouples placed inside SCR1 at mid-depth.

- TG_DPF_x: Gas temperature at DPF inlet
  Thermocouples placed just above the surface of the DPF brick.

The naming convention for radial position of the sensors are as follows:
1, 2, 3 correspond to radial distance from center. 1: 0 mm, 2 : ~70 mm, 3 : ~140 mm
U, D, L, R and its combinations correspond to directions up, down, left, right with respect to center in the direction of exhaust flow.

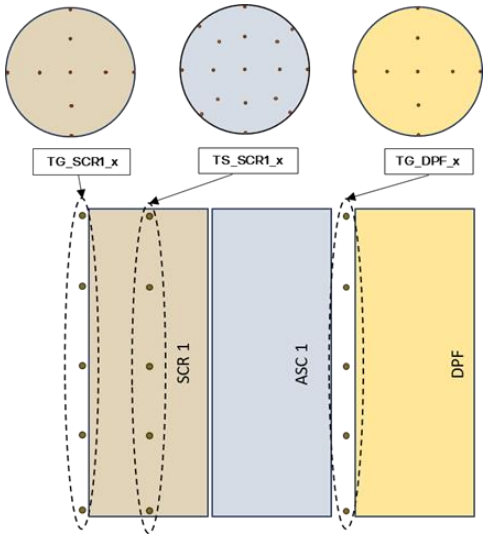

Figure 3.22 SCR1 and DPF thermocouples in engine test

The pipe routing to the diffuser cone was kept as straight as possible to minimize flow separation seen in the air flow rig tests. To improve the flow distribution before the diffuser cone, a large pressure drop like a DPF core would have been ideal. We saw earlier that temperature and flow maldistributions were present in the silencer inspite of having a DPF after the SCR1 and ASC1 blocks. Using a similar DPF core at the diffuser inlet could have improved the flow distribution because of a higher pressure drop. This is because the fluid velocity at the diffuser inlet is much higher due to the smaller cross-section, and pressure drop is proportional to the square of fluid velocity.

However, having a large pressure drop there would significantly change the operating conditions for the engine, and was thus ruled out as an option. Instead a mixer device was installed before the diffuser inlet to mix the inlet flow better and introduce turbulence in the form of smaller eddies to reduce flow separation at the diffuser wall. This device was repurposed from a mixer in the urea mixing chamber before the second SCR unit in the silencer.

Figure 3.23 Mixer installed upstream of diffuser inlet

Heater power in the tests here was maximum allowed power as recommended by the heater supplier. This was based on exhaust mass flow, and exhaust gas temperature measured at SCR1 inlet with the TE09 sensor. A condition was added to only use the heater when TE09 was less than 200°C.

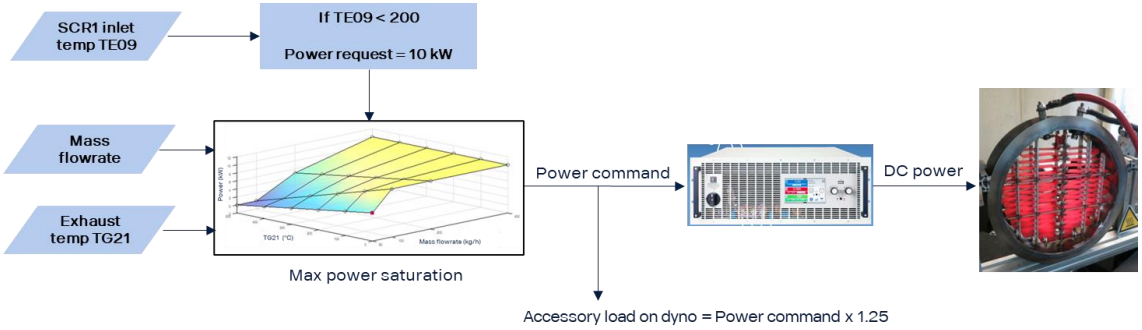

Figure 3.24 Heater power control flowchart

For low load and idling, it would have been better to regulate heater power with a proportional-integral controller to reduce oscillations but this was not possible to implement at the time. A proportional controller using a lookup table was tried but the behavior was found to not be very different from the maximum allowed power control because the output of the maximum allowed power lookup table is already proportional.

In a vehicle, power drawn by the heater would likely be drawn from the alternator with approximately 80% efficiency. To simulate this in the tests, the power drawn by the heater was multiplied with 1.25 and added as alternator load. For example, heater power of 8 kW translates to 10 kW of additional alternator load. This was however, found to not have worked perfectly in the tests. A hidden condition elsewhere in the test cell control code only added this simulated alternator load if it was less than 10 kW. Effectively, the additional load was only added when heater power was less than 8 kW.

For the test runs performed, requested heater power reduces to less than 8kW after some time because of the maximum allowed power lookup table as exhaust temperature increases. Until then, the energy for powering the heater was ‘free’. To account for this, the fuel consumption figures shown include additional fuel calculated by multiplying the ‘free’ energy with specific fuel consumption.

3.3.2 Results

3.3.2.1 Steady state

The distribution of a flow variable (temperature, velocity) can be defined by a uniformity index (UI) which gives the deviation of the variable from the mean value of the flow variable at a plane, and is described the formula below (ANSYS, 2024):

$$\gamma_a = 1 - \frac{1}{2}\left(\frac{\sum_{i=1}^{n} |\phi_i - \overline{\phi_a}| A_i}{\overline{\phi_a} \sum_{i=1}^{n} A_i}\right) \tag{3.1}$$

Here, ϕ_i is the measured value of the flow variable, $\overline{\phi_a}$ is the area-weighted average of the flow variable defined as:

$$\overline{\phi_a} = \frac{\sum_{i=1}^{n} \phi_i A_i}{\sum_{i=1}^{n} A_i} \tag{3.2}$$

Here, temperature is the flow variable being studied. UI ranges from 0 to 1. As an example, a relative deviation of 20% from the mean will give a UI of 0.9.

Since this formula for UI shows absolute deviations and not whether it is higher or lower than the mean value, a relative temperature ratio is used to plot the temperature distributions defined by the formula:

$$Relative\ temperature\ ratio = \frac{\phi_i - \overline{\phi_a}}{\overline{\phi_i}} \tag{3.3}$$

The temperature distributions at SCR1 inlet, SCR1 solid, and DPF inlet for 300 kg/h at steady state with and without the mixer device at 8 kW heater power are shown in Figure 3.25 and Figure 3.26. The same for 600 kg/h and 8 kW heater power are shown in Figure 3.27 and Figure 3.28.

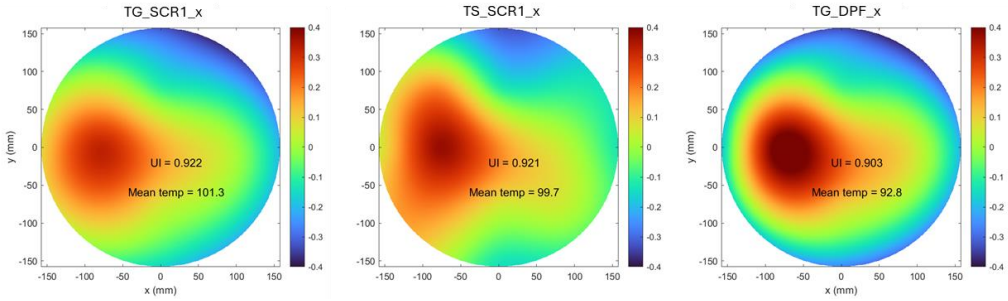

Figure 3.25 Relative temperature ratios at 300 kg/h and 8 kW with mixer

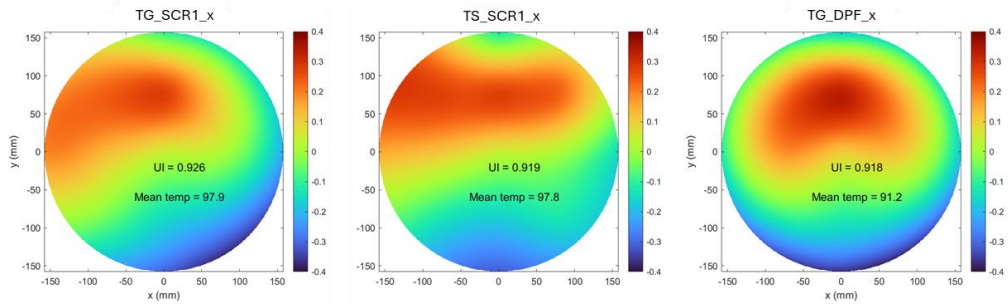

Figure 3.26 Relative temperature ratios at 300 kg/h and 8 kW without mixer

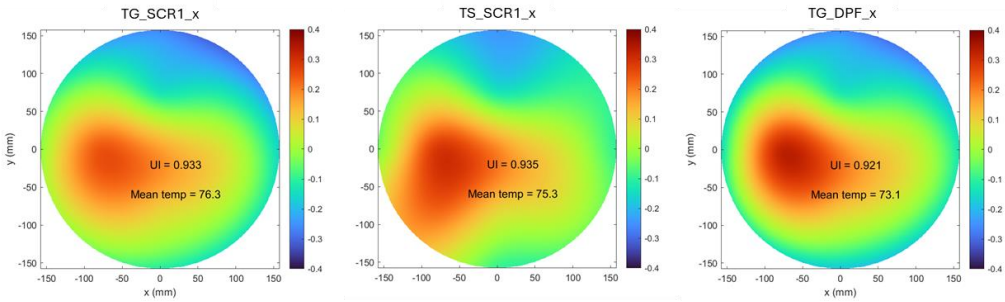

Figure 3.27 Relative temperature ratios at 600 kg/h and 8 kW with mixer

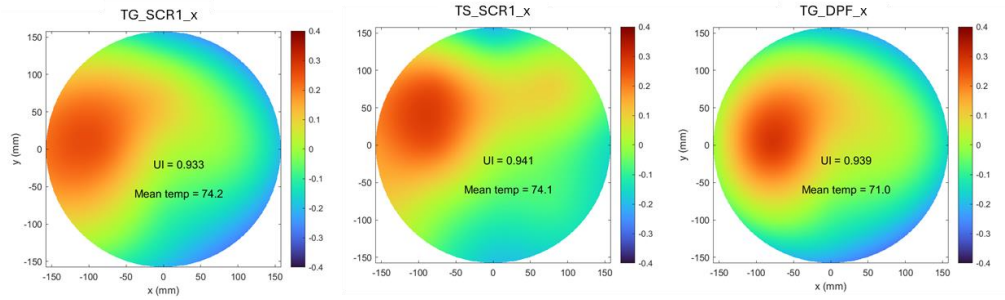

Figure 3.28 Relative temperature ratios at 600 kg/h and 8 kW without mixer

In both flow rate cases, the UI is slightly worse with the mixer device but the difference is less than 4% even for the largest UI deviation i.e., temperature distribution before DPF for 600 kg/h. As a trend, there is a localized hotspot close to the center of the plane and slightly offset to the left. The left offset could be explained by the bend towards the left in the pipe routing before the diffuser causing a left biased flow separation and recirculation zone before the heater and consequently a hotter than average region. A mixer design with more cross-mixing may have worked better but this could not be tested at the time.

The maximum power that could be drawn from the heater was 9 kW in this test setup as well, due to non-uniform heating of the heater band mentioned in Section 3.2.2.

3.3.2.2 Cold WHTC

Using the heater reduces the time to start dosing significantly for both modes FC and TM (first 600s of mode-free operation) as shown in Figure 3.29. In mode TM, due to the higher turbo outlet temperatures, heat losses in the diffuser are higher than in FC, resulting in the reduced time to dosing with heater not being much lower than the FC case with heater.

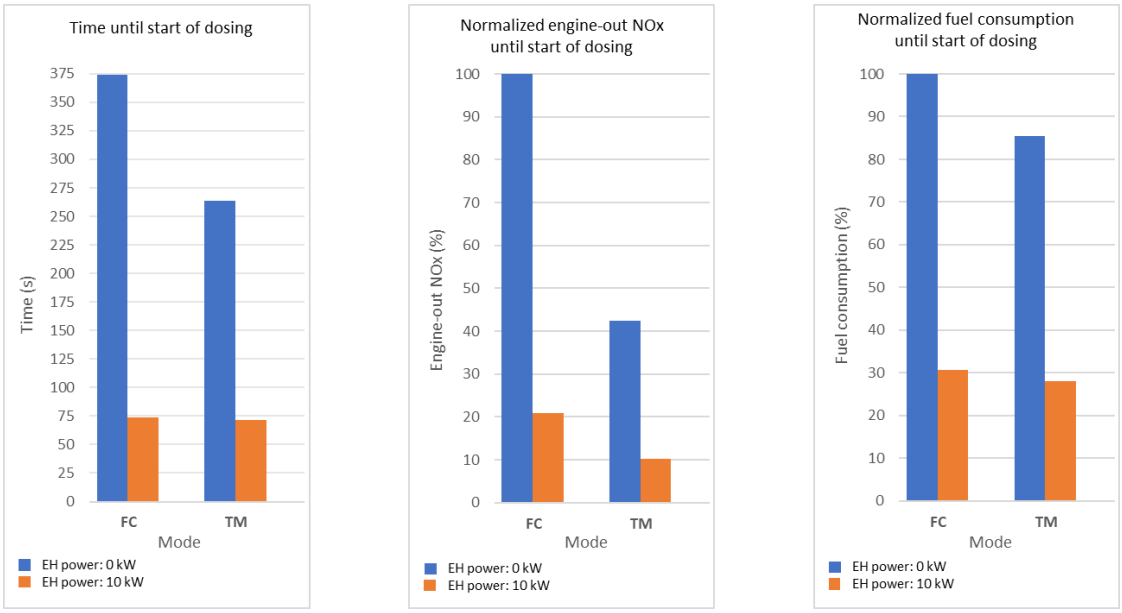

Figure 3.29 Time, engine-out NO_X and fuel consumed until start of dosing in cold WHTC

Until start of urea dosing, engine-out NO_X emissions are released from the tailpipe without being treated, and reducing this time is crucial in reducing NO_X emissions over the whole cycle. Engine-out NO_X is lowest when using the heater with mode TM. This is expected because in mode TM, engine-out NO_X is low and the time to start of dosing is lower. In addition, due to the lower time to start of dosing, fuel consumption is lowest too when using the heater with mode TM, even though TM is a less fuel efficient mode than FC.

Effectively, using engine-based exhaust heating together with the heater is the best compromise for NO_X and fuel economy for reducing time to start dosing among the cases tested here.

Comparing temperature traces in the beginning of a WHTC for modes FC and TM, we see that there is a large difference in TG21 and TE09 temperatures when the heater is not used. This difference is higher in mode TM because of larger heat losses at higher turbocharger outlet temperatures.

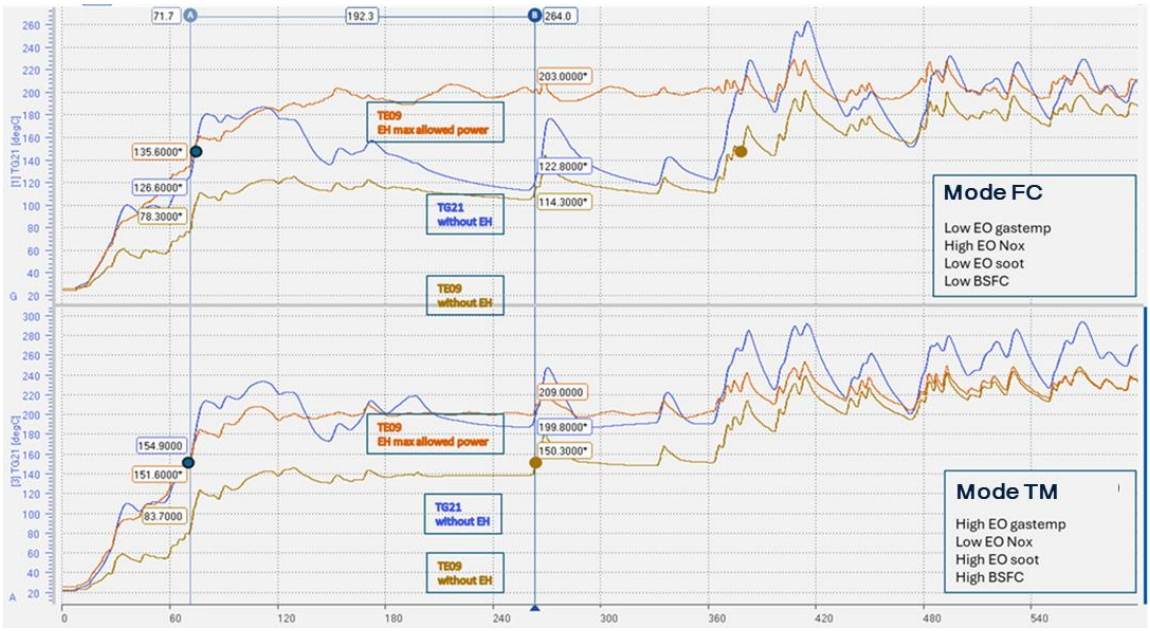

Figure 3.30 Temperature trace for 600s of cold WHTC

In the first 74 seconds of the cycle, it can be seen that using the heater brings the SCR1 inlet temperature back to the original turbo outlet temperature. Effectively, here the heater is only replacing the heat losses in the diffuser, heater body and pipes and reducing time to dosing to close to what it would have originally been.

This can be visualized by Sankey diagram in Figure 3.31 showing energy flow between the turbo outlet and SCR1 inlet for the first 74 seconds of the mode FC case. Since this was for the first 74 seconds of the cycle, some part of the losses can be attributed to heat up the added thermal inertia of the diffuser, heater body and pipes.

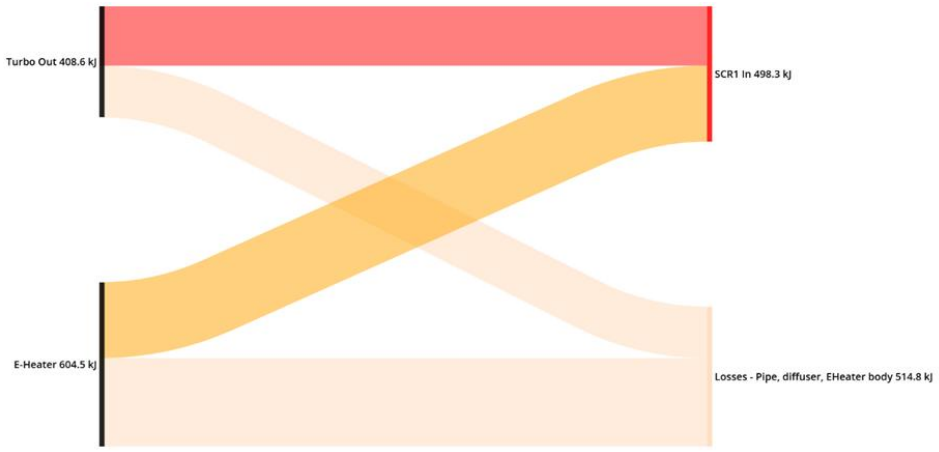

Figure 3.31 Energy flow between turbocharger outlet and SCR1 inlet for 74s of cold WHTC

Over the whole cycle, this distribution of heat flow is not as severe. However, as seen in the Sankey diagram in Figure 3.32, little more than half of the heat losses between turbo outlet and SCR1 inlet are replaced by the heater.

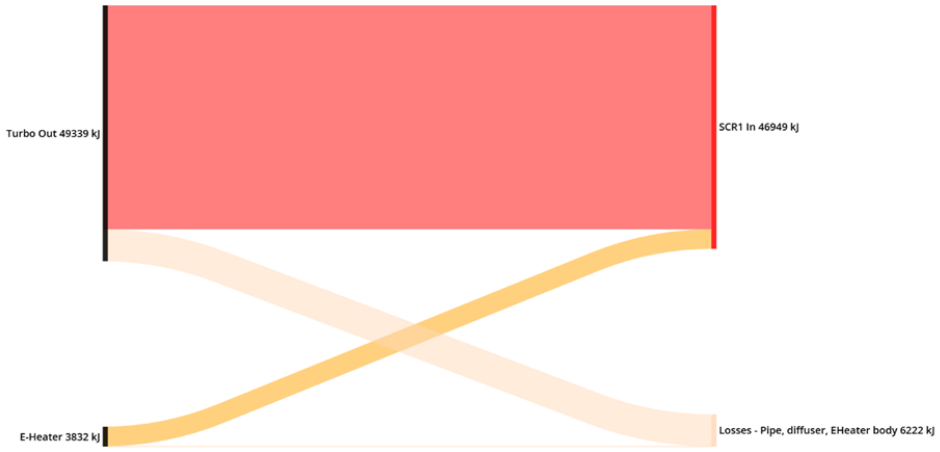

Figure 3.32 Energy flow between turbocharger outlet and SCR1 inlet in cold WHTC

Over the whole cycle, using the heater reduced the tailpipe NO_X emissions by 29% when operating in mode FC as seen in Figure 3.33. There is a difference in engine-out NO_X in the FC cases but the reduction at tailpipe with heater is still expected to be more than 24% if both FC cases had the same engine-out NO_X. In mode-free operation, the reduction with heater is only 7%. This is because of the lower total engine out NO_X emissions, and shorter time to start dosing in mode-free operation.

In the mode TM case, the tailpipe NO_X is not significantly lower than mode-free even though it runs in a lower engine-out NO_X mode because most of the cumulative tailpipe NO_X was released in the first 65 seconds before urea dosing started. The additional fuel penalty from using the heater is 2.5% in mode FC and 1.2% in mode-free. However, using the heater in both cases is still atleast 7% more fuel efficient than running the whole cycle in mode TM.

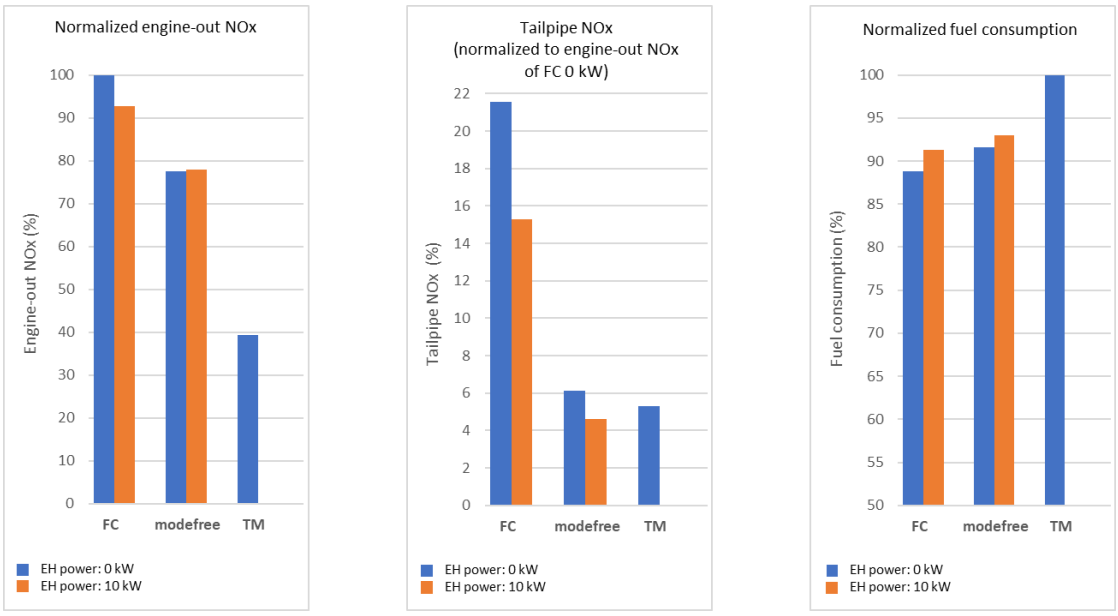

Figure 3.33 Engine-out NO_X, tailpipe NO_X and fuel consumed in cold WHTC

In earlier tests with a similar engine operating mode-free and a standard exhaust aftertreatment setup, the tailpipe NO_X value over the cycle is equal to that of the

mode-free with heater case here. This once again can be attributed to the previous argument that the heater was only replacing additional heat losses in this installation. Even with the heater in mode FC, the tailpipe NO_X value is significantly higher than mode-free with or without heater. Even though time to start of dosing was reduced to around 70 seconds in both FC and mode-free cases with heater, the mode-free case continues in the low engine-out NO_X mode TM until about 600 seconds which results in the tailpipe NO_X emissions over the cycle being much lower.

What this means is that even though the heater is able to reduce time to dosing significantly, it needs to be combined with running in a low engine-out NO_X mode to meet emission limits.

3.3.2.3 Low load cycle

In a low-load cycle (LLC) of average power 12 kW, similar losses as in the WHTC are seen between turbo outlet and SCR1 inlet.

In mode FC, turbo outlet temperature does not reach the minimum dosing temperature even after half an hour. SCR1 inlet temperature would take roughly 1.5 hours to reach the dosing temperature. Using the heater brought this down to 100s. In mode-free operation, minimum dosing temperature is reached in about 260s, and using the heater brings it down to 75s. Here, turbo outlet temperature reaches 150°C in about 75s, which means once again the heater is effectively replacing heat losses.

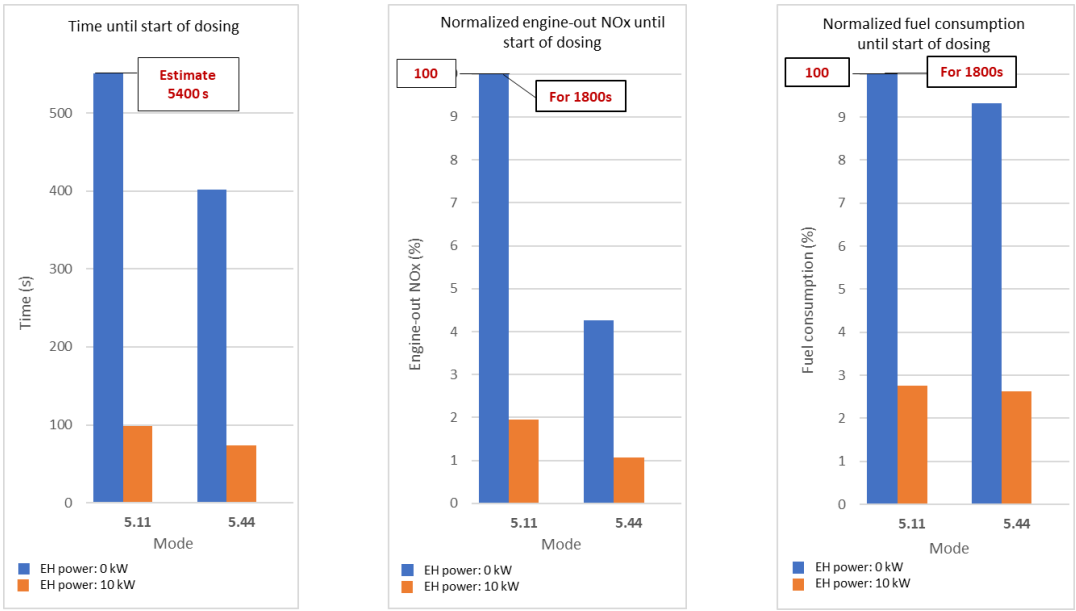

Figure 3.34 Time, engine-out NO_X and fuel consumed until start of dosing in LLC

Similar to WHTC, engine-out NO_X and fuel consumption until start of dosing is lowest in the TM with heater case. Here too, using engine-based exhaust heating together with the heater is the best compromise for NO_X and fuel economy for reducing time to start dosing among the cases tested here.

For half an hour of the low load cycle, using the heater reduced tailpipe NO_X emissions by 37% in mode FC. There were discrepancies in NO_X measurements in the

FC without heater case but the engine-out NO_X is expected to be the same as that in FC with heater. Since temperatures were too low to start dosing, tailpipe NO_X is also expected to be the same as engine-out NO_X. In mode-free operation, the reduction with heater is only 6%. The additional fuel penalty from using the heater is 20% more in mode FC and 10% more in mode-free. The penalties are higher in the low load cycle as compared to WHTC because the additional engine load due to the heater compared to the average power for the cycle is higher in the low load cycle than in WHTC. Similar to WHTC, even with the heater in mode FC, the tailpipe NO_X value is significantly higher than mode-free with or without heater.

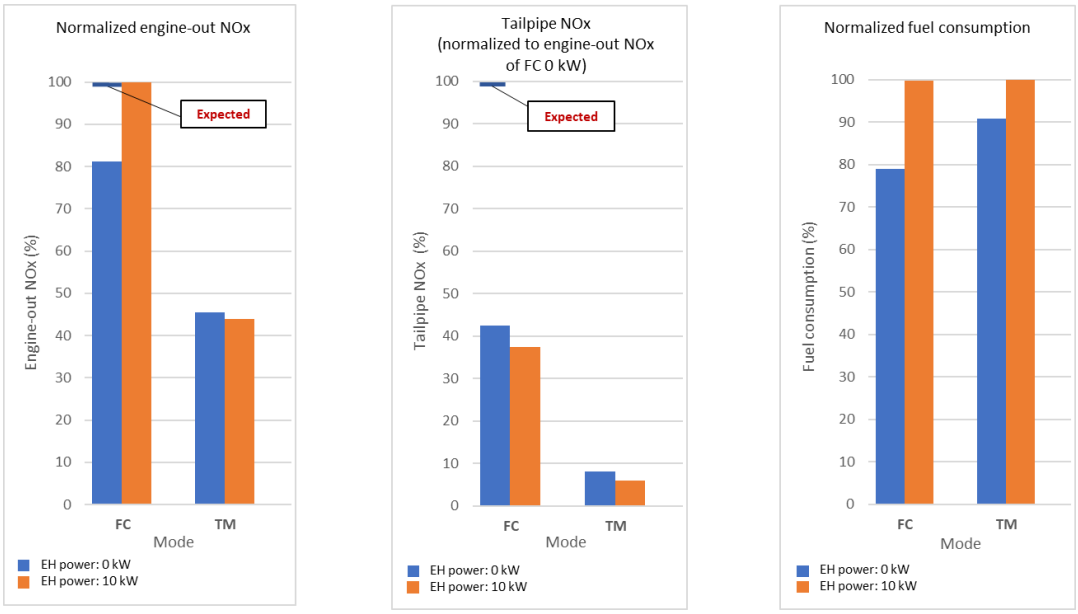

Figure 3.35 Engine-out NO_X, tailpipe NO_X and fuel consumed in LLC

Here too, even though the heater is able to reduce time to dosing significantly, it needs to be combined with running in a low engine-out NO_X mode to meet emission limits.

3.3.2.4 Idle

During idling from a cold start, the heater significantly reduces time to start dosing. In mode FC, turbo outlet and SCR1 inlet temperatures do not reach the minimum dosing temperature even after half an hour. It is uncertain how long it would take, if it does at all. Using the heater brought the time to start dosing down to 135s.
In mode-free operation, turbo outlet temperature reaches 150°C in about 156s but SCR1 inlet temperature only reaches dosing temperature after 885s. Using the heater brought this also down to 135s.

Interestingly, here, engine-out NO_X is higher in the mode-free cases than in FC. This was found to be because in mode-free operation (TM here) at idle, exhaust brake along with cam phasing is used to increase exhaust temperature. But in this engine calibration, lambda is severely lowered at this condition increasing NO_X emissions. Fuel consumption for the with heater cases could not be calculated. The added engine load due to the heater was not correctly added during these cycles, and calculating it based on specific fuel consumption for such low loads showed large discrepancies.

However, it is interesting that even with mode-free operation only run for half the duration as FC, it still has higher fuel consumption. Because of this and the low engine-out NO_X, using the FC mode with heater to reach dosing temperature quickly at idle could be potentially more fuel-efficient than mode-free with heater.

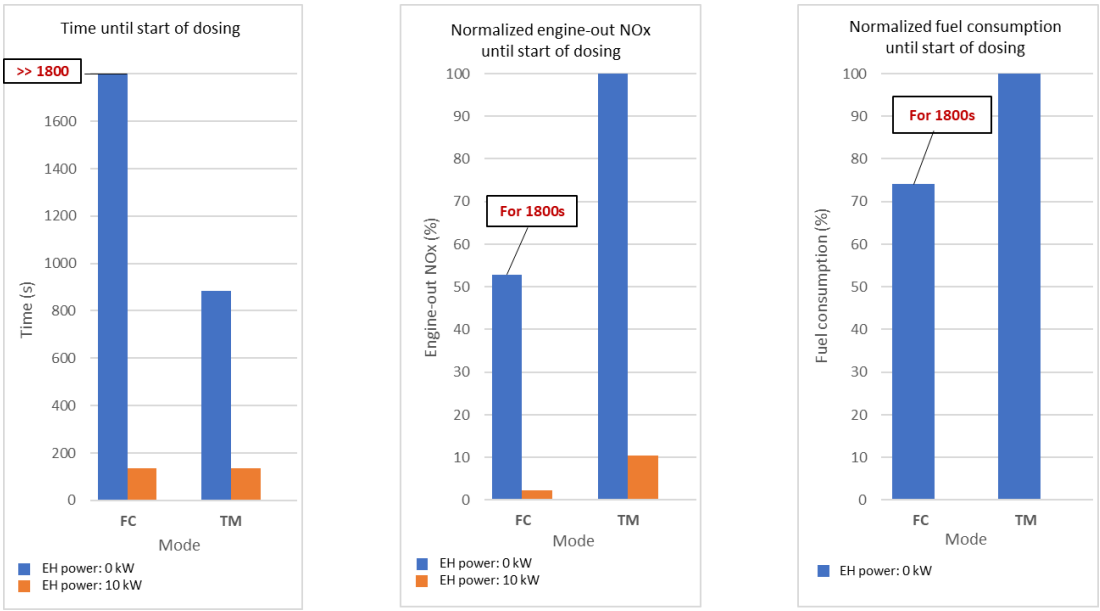

Figure 3.36 Time, engine-out NO_X and fuel consumed until start of dosing at idle

For half an hour of idling, using the heater reduced tailpipe NO_X emissions by 5% in mode FC. In mode-free, the reduction was 17%. Note that dosing on SCR1 was not active in both the mode-free cases here due to a condition in the software logic. Based on other tests, it is estimated that tailpipe NO_X in the mode-free cases would have been 40% lower if dosing on SCR1 was active. Although it could not be measured, use of the exhaust brake and cam phasing in mode TM was noisier than in mode FC where they were not used.

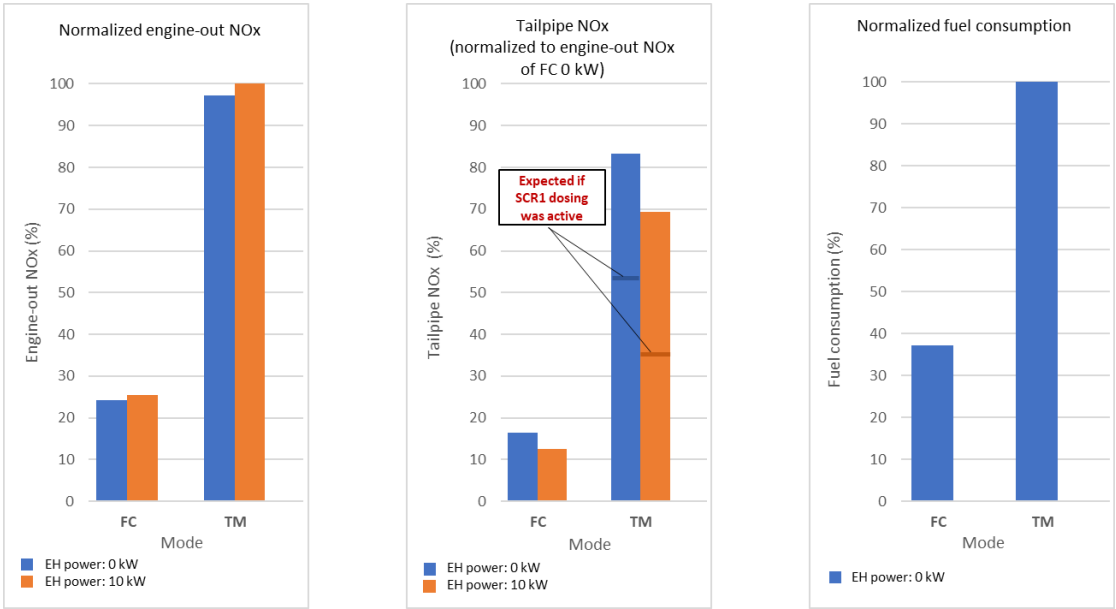

Figure 3.37 Engine-out NO_X, tailpipe NO_X and fuel consumed at idle

From the results at idle, operating the heater in mode FC is the best case for reducing NO_X but the fuel penalty is unknown. Additionally, this would allow for quieter operation.

The heater control method used here cycles the heater on and off when the temperature at TE09 is around 200°C. Although it could not be measured in this test, this will likely cause the fuel consumption to be higher due to the engine load fluctuating constantly. A more constant heater power using a better control method would potentially work better here.

A test was also performed by preheating the heater with 9 kW of power for 25s before idling in mode FC. The mean value for the thermocouples at SCR1 inlet showed a 25s difference in time to 150°C once the engine started idling. In this test, emission measurements could not be performed but NO_X reduction is expected with preheating due to the reduced time to start of dosing. If this energy was to be drawn from the battery with 80% efficiency, it would be 11.25 kW drawn from the battery for 25s. For a 24 V electrical system, this would be 469A of current and 3.26 Ah of energy drawn from the battery. Truck batteries of this size typically have above 160 Ah of capacity, and cold cranking amperage of 800 A. So preheating can be used without needing larger batteries.

To reach a turbocharger outlet temperature of 150°C in mode TM without heater takes two minutes and uses an extra 68 g of fuel as compared to the mode FC without heater case. The actual heat added to the exhaust gas is only equivalent to an average power of 3.2 kW. But this additional amount of fuel contains 2.9 MJ of energy equivalent to a theoretical 24 kW of average power. If this additional fuel was instead oxidized over a DOC, atleast 14 kW of heat could be generated assuming a conversion efficiency of 60% at 260°C. The light-off temperature could be achieved by preheating an electrically heated DOC before engine start.

3.4 1-D simulation

The commercial software AVL Cruise M was used to perform simulations of a 1D kinetic model of an exhaust aftertreatment system with an electric heater. A model previously made as part of a master thesis (Sabuco, 2021) was used as a base with some adjustments. The base model uses time-varying gas composition, temperature and mass flow from engine outlet measurements during test cycles as the inlet boundary conditions to the aftertreatment system model. Chemical reactions of the catalysts, and temperature and pressure of the complete Euro 6 system were calibrated using physical test data. However, this model does have limitations, among which are that reactions were modeled using surface reaction models, gas flow was considered perfectly uniform in the radial direction, the test data used for verifying simulation results were mainly intended for NO_X and ammonia slip, and that discrepancies were seen for high mass flow rates.

3.4.1 Setup

Due to differences in software versions, the base model had to be rebuilt after some troubleshooting to make it functional again. It was also found to be based on a different silencer having a larger DPF cell wall thickness and shorter SCR2 bricks.

Simulations using data from earlier tests verified that this model worked well to simulate temperatures and NO_X after the first and second SCR units.

The new model was updated with component sizes matching the installation used in the tests, and an electric heater component which was recently made available in the Cruise M standard component list. The heater component is based on a honeycomb catalyst with a heating functionality, and dimensions were updated to match those of the heater used in the tests. To make the heated honeycomb in the model functionally similar to the heater band, simulations with constant mass flow and heater power were performed to compare the outlet gas temperature with results from the flow rig test, and heater substrate temperature with estimates based on Figure 3.5. Changes to the open frontal area and hydraulic diameter settings made the biggest difference, but the actual values of open frontal area and hydraulic diameter from physical measurements of the heater worked well.
A bug in the new heater component caused the software to corrupt project files and results from all the simulations performed, and simulations had to be repeated after a fix was provided by AVL.

The diffuser cone used in the tests was added to this model as multiple pipe lengths of increasing diameter. This was only to include the thermal inertia and heat losses due to surface area of the diffuser as the flow separation and recirculation effects would not be simulated in 1D.

Simulations were performed using engine-out species data measured by the FTIR and turbocharger outlet temperatures for the mode FC cases in the engine tests.
These were first run with actual dosing values recorded in the tests as input for the DEF dosing points in the model. This was then repeated with a simplified dosing strategy based on temperatures at the TE09 and TE11 measurement points. The dosing strategy used is described below:

- Dosing point 1:
  if TE09 > 150

if TE11 > 180

ANR = 0.4

else

ANR = 1.1

else

ANR = 0

- Dosing point 2:
  if TE11> 180

ANR = 1.1

else

ANR = 0

Simulations with heater power using the same logic for maximum allowed power as in the engine tests were performed using the simplified dosing strategy and actual dosing values from the test cases where the heater was used. The NO_X reduction using the simplified strategy was very close to that with actual dosing values.

A problem seen in all the simulations performed was that the temperature after the DPF increased much slower than in the flow rig and engine tests. This also meant that

NO_X reduction in the second SCR units was significantly less in simulations. Adjustments to the model by correcting the DPF cell wall thickness, component sizes and thermal inertia multipliers showed some improvement but still significantly different from test data. This was attributed to the flow distribution problem causing warm exhaust gas to pass through without evenly heating the DPF and components before it as mentioned in section 3.2.2. In simulations, flow maldistribution is not accounted for, resulting in temperatures after the DPF to rise slower.

3.4.2 Results

3.4.2.1 Cold WHTC

Simulations were performed for a cold WHTC operating in mode FC. DEF dosing was based on the 0.4/1.1 ANR strategy. Heater power control strategy was the same as that used in the tests.
In both with and without heater cases, simulations showed higher tailpipe NO_X as compared to tests. But for both test and simulation, using the heater showed a 6% reduction. NO_X at SCR1 outlet was similar in test and simulation. This is because the temperature at SCR1 in the simulations follow the test data quite well. However, since the temperature after the DPF rose faster in the test, NO_X reduction at SCR2 started earlier.

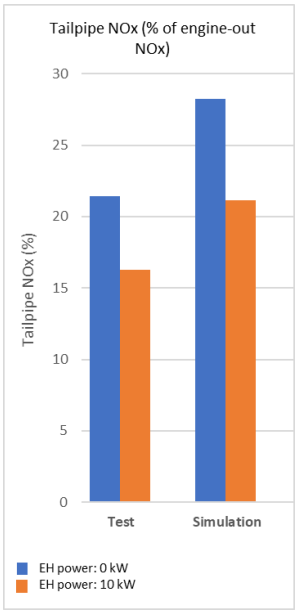

Figure 3.38 Comparison of tailpipe NO_X in test and simulation for cold WHTC

A simulation without the diffuser cone was performed to see the difference that could be made if the heat losses before the heater were minimized. NO_X at SCR1 outlet was similar but NO_X at tailpipe was 6% less without the diffuser for both with and without heater cases. Electrical energy required by the heater during this cycle was 34% lower without the diffuser.

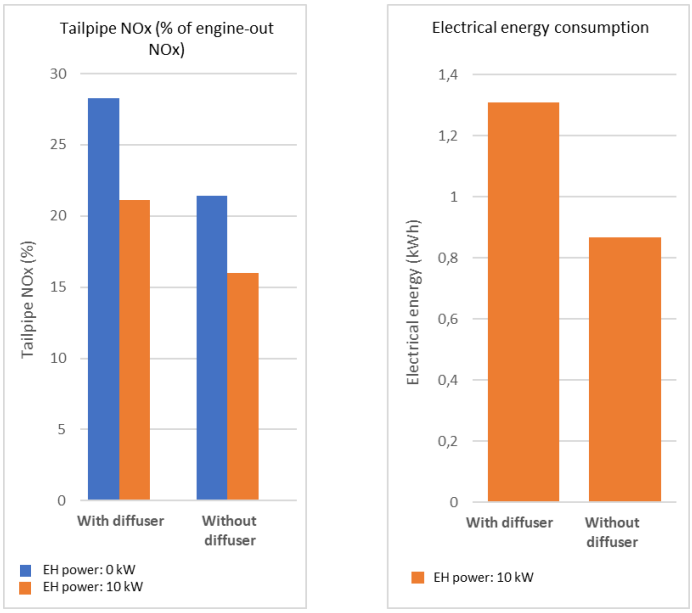

Figure 3.39 Comparison of tailpipe NO_X and heater energy consumption with and without diffuser for cold WHTC

To meet an acceptable target for tailpipe NO_X, a value equivalent to 5% or lower in Figure 3.39 is required. This was met by the modefree with heater case in the test. The limiting problem here is that as soon as TE11 reaches 180°C, dosing at SCR1 reduces to ANR 0.4, so that SCR2 can perform the bulk of the NO_X reduction. Although 150°C is sufficient to start NO_X reduction, the SCR unit only reaches peak efficiency above 240°C.

Simulations were performed with increasing target temperatures, changing the target from TE09 to TE11, and with double the heater power. All of these improve tailpipe NO_X by increasing the average temperature at SCR2 inlet over the cycle, but only the 20kW cases are sufficient to keep it above 240°C and reduce the NO_X level to less than 5%. Of these 20 kW cases, using TE11 for target requires lower electrical energy over the cycle. However, this is still more than 6 times the energy consumed by the heater in the engine test.

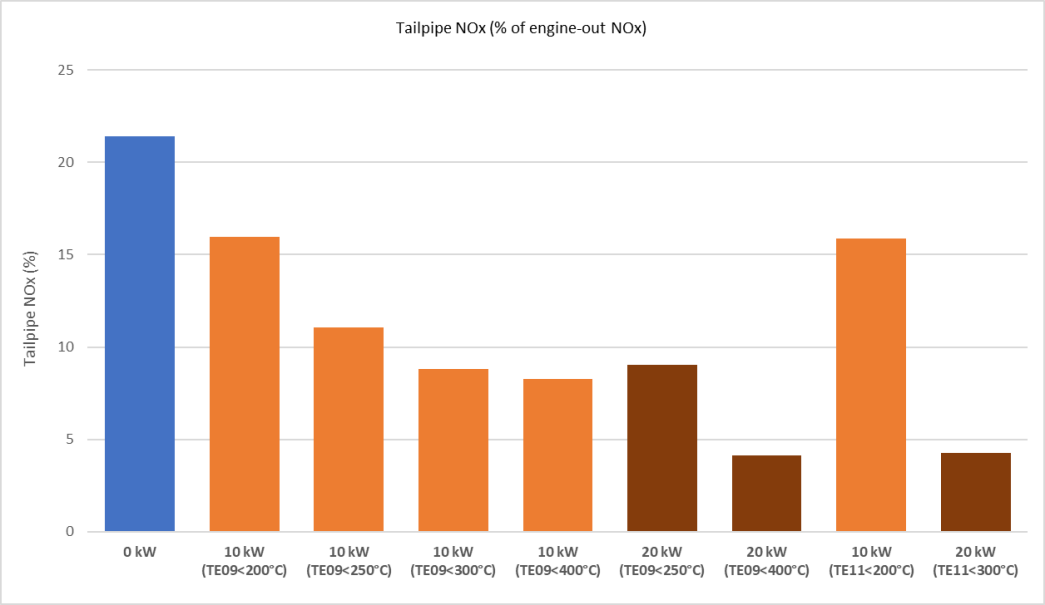

Figure 3.40 Comparison of tailpipe NO_X with different heater strategies for cold WHTC

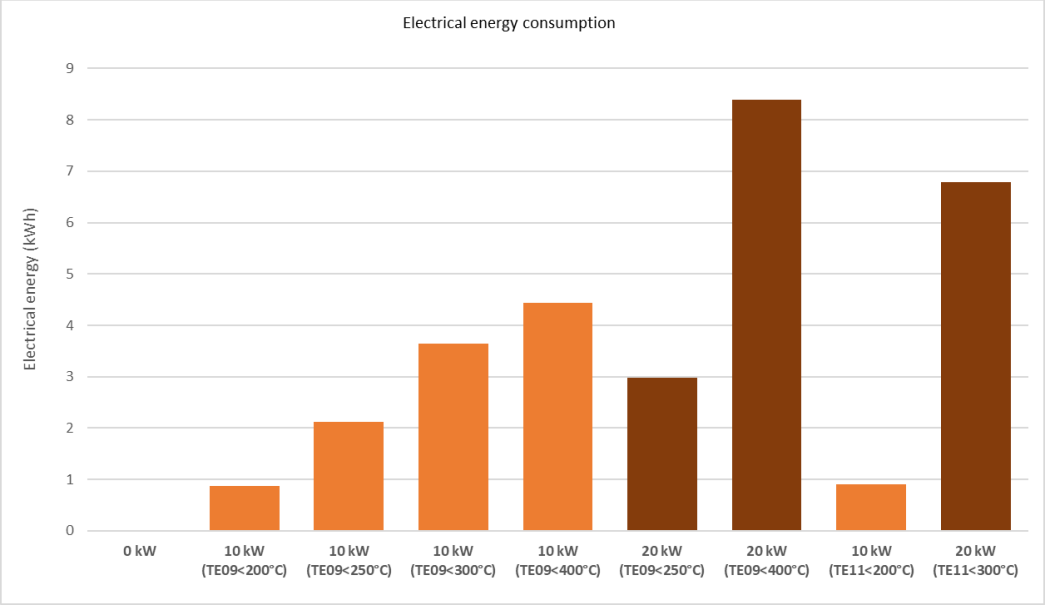

Figure 3.41 Comparison of heater energy consumption with different heater strategies for cold WHTC

3.4.2.2 Low load cycle

Simulations were performed for 30 minutes of the low load cycle operating in mode FC.

In the case without the heater, dosing temperatures are not reached during the cycle so no NO_X reduction takes place. In the case with heater, simulation showed higher tailpipe NO_X as compared to the test. This is attributed to the temperature after DPF rising faster in the test, and subsequently earlier NO_X reduction in SCR2.

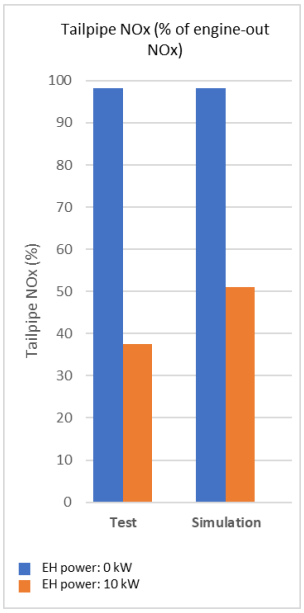

Figure 3.42 Comparison of tailpipe NO_X in test and simulation for LLC

A simulation without the diffuser cone showed tailpipe NO_X 5% less without the diffuser for both with and without heater cases. Electrical energy required by the heater during this cycle was 12% lower without the diffuser.

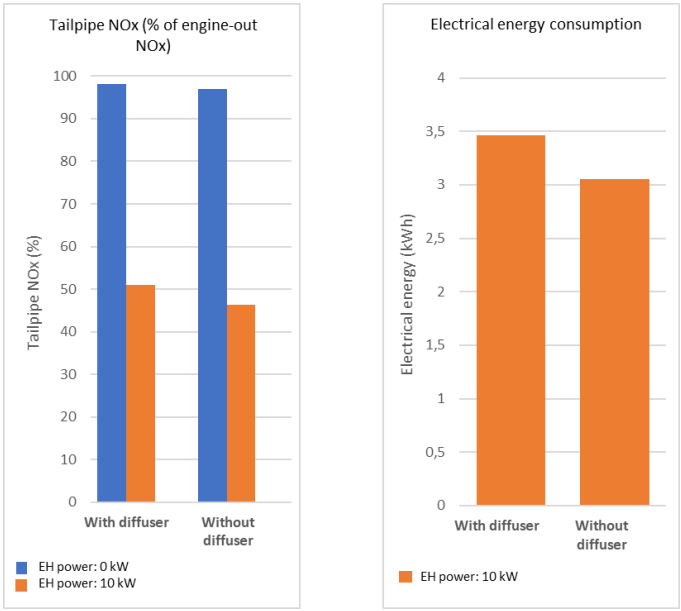

Figure 3.43 Comparison of tailpipe NO_X and heater energy consumption with and without diffuser for LLC

To obtain the same tailpipe NO_X as the modefree without heater case in the test, a value equivalent to 11% or lower in Figure 3.42 is required. Simulations were performed with increasing target temperatures, changing the target from TE09 to TE11, and with double the heater power. However, even with 20 kW of power and using TE11 for target temperature only reduces this to 20% and requires almost 3 times the energy consumed by the heater in the engine test.

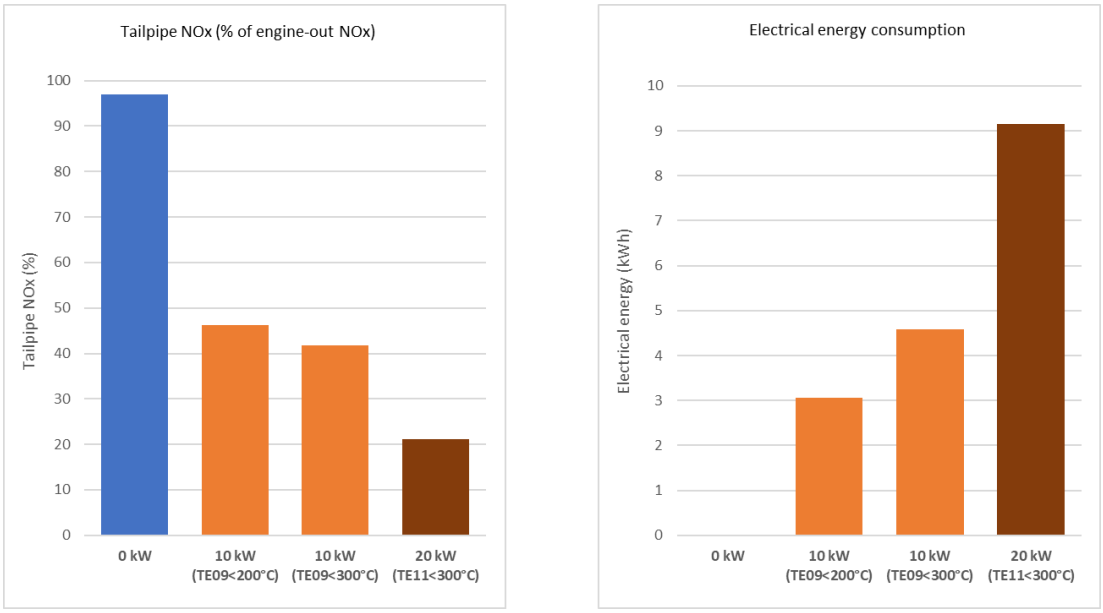

Figure 3.44 Comparison of tailpipe NO_X and heater energy consumption with different heater strategies for LLC

3.4.2.3 Idle

Simulations were performed for 30 minutes of idle operating in mode FC.
In the case without the heater, dosing temperatures are not reached during the cycle so no NO_X reduction takes place. In the case with heater, simulation showed 5% lower tailpipe NO_X as compared to the test. At these engine-out NO_X values, the amount of DEF injected at the first dosing point is very small and not injected at a constant rate because the injector has a lower threshold for injection rate. Additionally, the temperature at the injection point is lower than 80°C and the flow rate is very low for proper mixing so most of the DEF injected was likely being deposited on the pipe walls. This is seen in NO_X values after SCR1 being 45% higher in test as compared to simulation.

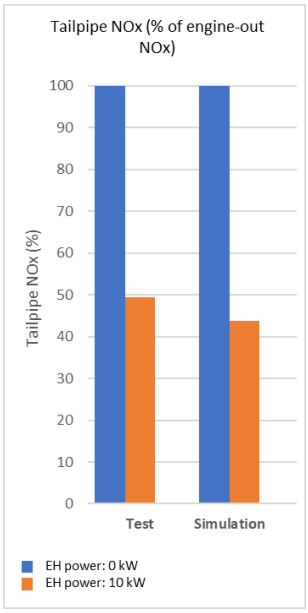

Figure 3.45 Comparison of tailpipe NO_X in test and simulation for idle

A simulation without the diffuser cone showed no difference in tailpipe NO_X without the heater because of no dosing, and less than 1% with heater. Electrical energy required by the heater during this cycle was 15% lower without the diffuser.

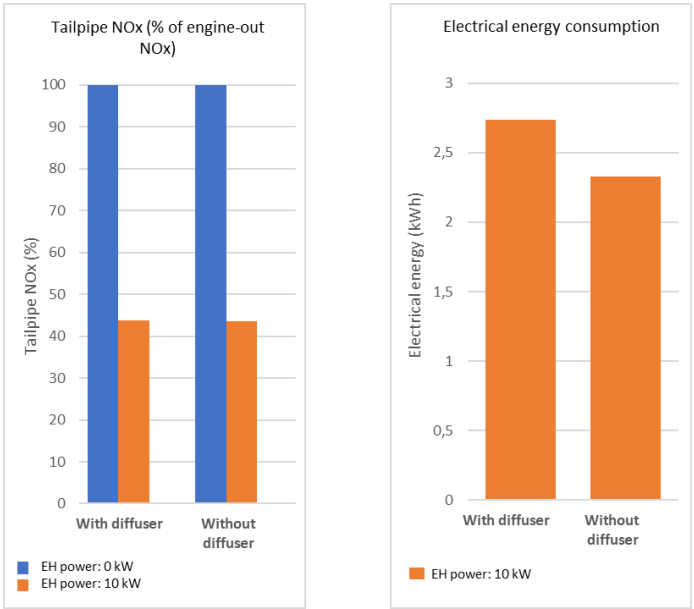

Figure 3.46 Comparison of tailpipe NO_X and heater energy consumption with and without diffuser for idle

To meet an acceptable target for tailpipe NO_X, a value equivalent to 41% or lower in Figure 3.45 is required. This is easily met by a 10 kW heater if the target temperature at TE09 is increased to 250°C.

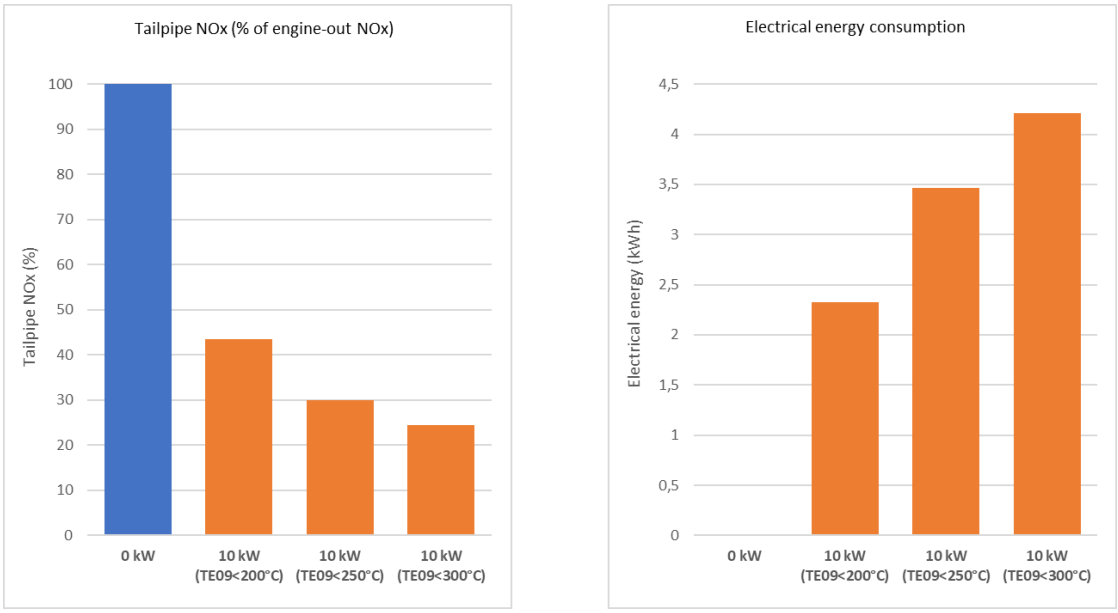

Figure 3.47 Comparison of tailpipe NO_X and heater energy consumption with different heater strategies for idle

3.5 Conclusions

An electric heater in the exhaust aftertreatment system can provide significant benefits to tailpipe emissions and fuel consumption. Integrating a heater into an existing aftertreatment system is simple in principle, but this evaluation shows that its performance is very sensitive to the installation.

The flow rig tests showed that higher heater powers translate to faster heatup of the SCR1 brick with diminishing gains beyond 7.5 kW. For low heater powers, the SCR1 brick heats up faster at lower flowrates but beyond 7 kW, higher flowrates heat up the brick faster.

In this installation, a large diameter heater was placed before SCR1 and required a large diffuser cone to accommodate the difference in pipe diameter. Flow separation due to a pipe bend and diffuser resulted in severe maldistribution of gas temperature and flow through the heater as seen in test and CFD simulation results. This maldistribution continues past SCR1, ASC and the DPF resulting in uneven heating of the catalysts. Straightening the flow into the diffuser does not reduce the maldistribution and can only be resolved by using flow guiding devices like vanes or a significantly large pressure drop.

Large heat losses and increased time to heatup of SCR1 were seen due to the surface area and thermal inertia of the diffuser. Radiative heat transfer from the heater to the diffuser upstream adds to the heat losses of the heater. Without these losses, lower tailpipe NO_X levels can be achieved with lower energy consumption. Using a mixer device at the diffuser inlet did not improve the temperature and flow maldistribution. Using a mixer design with better cross-mixing could potentially show better results.

In a cold WHTC cycle, a 10 kW heater is insufficient to meet NO_X emission requirements if operating in the high NO_X low fuel consumption mode.
However, in the low NO_X engine-based exhaust heating mode, a 10 kW heater shows a good compromise between NO_X emissions and fuel consumption. 1D simulations for the high NO_X low fuel consumption mode showed that if the heat losses due to the diffuser were not present, tailpipe NO_X could be 6% lower and heater energy consumption could be 18% lower. Using a 20 kW heater could reduce the tailpipe NO_X to meet emission limits even in the high NO_X mode but the fuel penalty would be worse than using engine-based exhaust heating.
Effectively, a heater alone is insufficient to reduce tailpipe NO_X to Euro 7 limits and requires some amount of operating in low engine-out NO_X modes.

In a low load cycle, a 10 kW heater is insufficient to meet NO_X emission requirements if operating in the high NO_X low fuel consumption mode. However, in the low NO_X engine-based exhaust heating mode, a 10 kW heater shows a good compromise between NO_X emissions and fuel consumption. Simulations for the high NO_X low fuel consumption mode showed that if the heat losses due to the diffuser were not present, tailpipe NO_X could be 5% lower and heater energy consumption could be 12% lower. Even though using a 20 kW heater could reduce the tailpipe NO_X to meet emission limits even in the high NO_X mode but the fuel penalty would be worse than using engine-based exhaust heating.

In idle, a 10 kW heater is sufficient to meet the NO_X emission requirement for clean idle when operating in the high NO_X low fuel consumption mode. Fuel penalty from using the heater is unknown but it is assumed to be lower than using engine-based exhaust heating. Additionally, using an electric heater instead of cam phasing and exhaust brake allows quieter idling. Preheating the heater before engine start can reduce time to start of dosing and consequently NO_X emissions.

In both idle and low load cycles, once the engine and aftertreatment system are warmed up, 4 kW is sufficient to maintain the minimum dosing temperatures of 150°C at SCR1 inlet.

When operating modefree, the time spent in mode TM was reduced when using the heater for all three engine test cycles. This means the time spent in high soot modes was reduced. This potentially reduces need for DPF regeneration.

The heater control strategy in the tests in this evaluation used maximum allowed power while SCR1 inlet temperature is below 200°C. Simulations have shown that increasing the target temperature and changing the target from SCR1 inlet to SCR2 inlet can improve cycle emissions.

Along with the heat losses and flow distribution problems mentioned earlier, the location of the heater is not ideal. Here, the heater is positioned downstream of the first dosing point while the temperature sensor for dosing control is downstream of the heater. This means that urea dosing starts even when gas temperatures at the dosing point are too low for effective evaporation and hydrolysis to ammonia. Additionally, urea coming into contact with the hot surface of the heater band (~800°C) can be oxidized forming NO_X. Although not investigated in this evaluation, these can result in urea deposits and insufficient NO_X conversion at SCR1. Using the heater and dosing only at the second dosing point until exhaust outlet temperatures are sufficiently high at the first dosing point could partly improve NO_X conversion at cold start.

If a large diameter heater with low backpressure is to be used, a potential solution is to integrate it into the silencer directly before the SCR1 brick with baffles and guide vanes to optimize the flow. The SCR1 brick can also be heated by radiative heat transfer from the heater band but there will still be radiative heat losses to the silencer shell on the upstream side of the heater band.

A smaller diameter heater in this aftertreatment layout will suffer less from flow maldistribution and radiative heat losses but there will be a fuel penalty due to the increased back pressure. Here too, the location of the heater is crucial. Having the heater close to the first dosing point would allow earlier dosing but there would be significant heat losses before the exhaust gases reach SCR1.

3.6 Future work

This thesis was a preliminary study into the performance of an electric heater in reducing NO_X emissions and the challenges associated with it. A major part of this project was the preparations involved in setting up tests with a heater for the first time in the organization. However, the learnings from this project will be useful for future investigations.

More investigations are required in understanding and solving the flow maldistribution problem that was found to be a major challenge in this project. 1D simulations have been found to work well but need to be supplemented with flow distribution data from 3D CFD studies to obtain results that are closer to those from physical tests.

If using an electric heater, it would be useful to investigate other aftertreatment system layouts that are better adapted for it. There is potential for better results if the engine-based exhaust heating and dosing control are adapted to having a heater in the installation as compared to the standard engine software used in these tests. There is also potential for lower energy consumption and emissions with better heater control logic than what was used in this evaluation.

In this thesis, only NO_X emissions were evaluated. A reduction in tailpipe HC emissions was noticed when using the heater but was not evaluated in detail. PM, N_2O and NH_3 are other relevant emissions that also need to be looked into for future studies.

4 References

ANSYS: *Fluent 2024R2 Theory Guide - 25.3.1.18. Uniformity Index*, 2024

Brodrick C.-J. et al. (2001): Truck Idling Trends: Results of a Pilot Survey in Northern California. *SAE Technical Paper 54*2001

Culbertson D. et al. (2016): A Simulation Study of Electrically Heating Diesel Exhaust. *SAE Technical Paper 262016-01-0927*, 2016

Culbertson D. et al. (2018): Exhaust Heating System Performance for Boosting SCR Low Temperature Efficiency. *SAE Technical Paper 52018-01-1428*, 2018

Culbertson D. et al. (2015): The Study of Exhaust Heating to Improve SCR Cold Start Performance. *SAE International Journal of Engines*, Vol. 8, No. 3, pp. 1187-1195, 2015

de Podesta M. et al. (2018): Air temperature sensors: dependence of radiative errors on sensor diameter in precision metrology and meteorology. *Metrologia*, Vol. 55, No. 2, pp. 229-244, 2018

Hamedi M. R. et al. (2021): Energy-efficient heating strategies of diesel oxidation catalyst for low emissions vehicles. *Energy*, Vol. 230, 2021

Infineum Insight. (2024): *The Euro 7 roller coaster*. Electronic Article, https://www.infineuminsight.com/en-gb/articles/the-euro-7-roller-coaster/

Jarrier L. et al. (2000): Warm-Up of a D.I. Diesel Engine: Experiment and Modeling. *SAE Technical Paper 322000-01-0299*, 2000

Jiao P. et al. (2017): Research of DPF regeneration with NOx-PM coupled chemical reaction. *Applied Thermal Engineering*, Vol. 110, pp. 737-745, 2017

Kim C. H. et al. (2012): Electrically Heated Catalysts for Cold-Start Emissions in Diesel Aftertreatment. *SAE Technical Paper 252012-01-1092*, 2012

Kubsh J. E., Brunson, G. W. (1996): EHC Design Options and Performance. *SAE Technical Paper 43960341*, 1996

Kumar A. et al. (2018): Reactor System with Diesel Injection Capability for DOC Evaluations. *SAE Technical Paper 532018-01-0647*, 2018

Küper P. F. et al. (1994): Ultra-Low Power Electrically-Heated Catalyst System. *SAE Technical Paper 44940465*, 1994

Li K. et al. (2024): Applications of Electric Heating Technology in Vehicle Exhaust Pollution Control. *Processes*, Vol. 12, No. 2, 2024

Lindemann B. et al. (2022): Electric Heater for Rapid Heating of the Exhaust Gas Aftertreatment System. *ATZheavy duty worldwide*, Vol. 15, No. 3, pp. 38-43, 2022

Majewski W. A. (2020): *Diesel Particulate Filters*. Electronic Article, https://dieselnet.com/tech/dpf.php

Majewski W. A. (2022): *Cellular Monolith Substrates*. Electronic Article, https://dieselnet.com/tech/cat_substrate.php

Majewski W. A. (2024a): *Diesel Oxidation Catalyst*. Electronic Article, https://dieselnet.com/tech/cat_doc.php

Majewski W. A. (2024b): *What Are Diesel Emissions*. Electronic Article, https://dieselnet.com/tech/emissions.php

Mendoza Villafuerte P. et al. (2021): Ultra-Low NOx Emissions with a Close-Coupled Emission Control System on a Heavy-Duty Truck Application. *SAE International Journal of Advances and Current Practices in Mobility*, Vol. 4, No. 2, pp. 602-609, 2021

Mendoza Villafuerte P. et al. (2022): Future-proof heavy-duty truck achieving ultra-low pollutant emissions with a close-coupled emission control system including active thermal management. *Transportation Engineering*, Vol. 9, 2022

Ravi S. S. et al. (2023): Impact of Modern Vehicular Technologies and Emission Regulations on Improving Global Air Quality. *Atmosphere*, Vol. 14, No. 7, 2023

Reşitoğlu İ. A. et al. (2014): The pollutant emissions from diesel-engine vehicles and exhaust aftertreatment systems. *Clean Technologies and Environmental Policy*, Vol. 17, No. 1, pp. 15-27, 2014

Romero C. A. et al. (2014): Energy Balance During the Warm-Up of a Diesel Engine. *30*2014

Sabuco P. (2021): *Exhaust aftertreatment system 1D model development using AVL Cruise M*. Master thesis, ESTACA, Paris, France, 2021

Shirizadeh B. et al. (2024): Climate neutrality in European heavy-duty road transport: How to decarbonise trucks and buses in less than 30 years? *Energy Conversion and Management*, Vol. 309, 2024

The Danish Environmental Protection Agency: *Close-coupled SCR systems for NOx abatement from diesel exhausts*, Odense, Denmark, 2021

Zavala B. et al. (2022): Fast Diesel Aftertreatment Heat-Up Using CDA and an Electrical Heater Between 1.2 and 5.0 kW. *Frontiers in Mechanical Engineering*, Vol. 8, 2022

DEPARTMENT OF MECHANICS AND MARITIME SCIENCES
MOBILITY ENGINEERING
CHALMERS UNIVERSITY OF TECHNOLOGY
Gothenburg, Sweden 2025
www.chalmers.se

CHALMERS
UNIVERSITY OF TECHNOLOGY